Calcium signaling components and their effect on synaptic morphology during neuronal development

BY

Raymond C. Caylor

Submitted to the graduate degree program in Molecular Biosciences and the Graduate Faculty of the University of Kansas in partial fulfillment of the requirements for the degree of Doctor of Philosophy.

_____
Chairperson – Dr. Brian D. Ackley

_____
Dr. Erik Lundquist

_____
Dr. Chris Gamblin

_____
Dr. Robert Ward

_____
Dr. John Kelly

Date defended: March 14, 2014

The dissertation committee for Raymond C. Caylor
certifies that this is the approved version of the following dissertation:

Calcium signaling components and their effect on synaptic morphology during neuronal development

_____
Chairperson – Dr. Brian D. Ackley

Date approved: March 14, 2014

Abstract

Along with regulating synaptic transmission, voltage-gated calcium channel (VGCC) function is responsible for a myriad of cellular outputs, ranging from gene expression to shaping synaptic morphology. Despite the morphological role of VGCCs, the proteins working downstream of VGCCs to regulate synaptic morphology remain mostly unknown, and their identification would provide insight into the shaping of synapses through calcium signaling.

Chapter I introduces the *Caenorhabditis elegans* VGCC subunits *unc-2* and *unc*-36 as regulators of D-type GABAergic neuromuscular junction morphology. In addition to synaptic defects found in single mutants, loss-of-function mutations in VGCC subunits, independent of neurotransmission, suppressed the enlarged synaptic areas resulting from mutations in the extracellular matrix protein nidogen (*nid-1*). Furthermore, time-lapse microscopy revealed UNC-2 function was required for proper synaptic dynamics that occurred during the L4 larval stage of organismal growth. Specifically, the dynamics observed in wild-type animals were slowed or absent in *unc-2* mutants. Since wild-type synapses undergo enlargement – increasing to areas similar to *nid-1* – and subsequently divide into two smaller puncta, we conclude UNC-2 is responsible for a temporal switch between synaptic stability and growth to add synapses during development.

In chapter III, I detail the characterization of the *calm-1* (ortholog of calmyrin), a gene encoding an EF hand protein that was identified in a *nid-1* suppressor screen. Double mutant analysis between *calm-1* and VGCC subunits suggests *calm-1* acts downstream of VGCCs to regulate synaptic morphology. This

result is the first to find a calmyrin protein that affects synapse morphology downstream of VGCCs. A calcium-dependent CALM-1 pulldown identified the intracellular scaffolding protein RACK-1 as a protein that may be targeted via VGCC/CALM-1 signaling. Similar to *nid-1, rack-1* mutants displayed abnormally shaped synaptic areas that were suppressed by *calm-1* mutants.

In conclusion, my genetic analyses suggest synaptic growth through VGCCs is normally inhibited by NID-1. But this inhibition is relieved during development to allow synaptogenesis to occur, commensurate with increases in organismal size, from the expansion and budding of existing synaptic connections. Thus, the cycling between synaptic adhesion and growth allows for a rapid and localized mechanism to add new synapses.

Acknowledgements

I would not have been able to make it through the numerous challenges of graduate school without the support of many people. First, I would like to thank my family for their constant love and encouragement. Despite there being some disconnect between their knowledge of what exactly I have been doing in graduate school, which I regret I did not try harder to ameliorate, they have always had complete faith and confidence in me; those short “I am proud of you” and “ I know you can do it” comments have provided me with much needed boosts of energy. To my parents, Andy and Terri, and my sister, Kristie, I love you and thank you so much.

I would like to thank my mentor, Dr. Brian Ackley. I have grown so much as a scientist and a person since joining the Ackley lab. Thanks for your patience, help and confidence to allow for the freedom to develop my own project. I consider myself lucky to have ben able to learn from you, and I look forward to using the skills I have acquired from my time in lab in the future. I also want to thank Dr. Martin Hudson for all the insightful conversations about science and life that have helped my growth as a person. Dr. Erik Lundquist also deserves many thanks for his advice and insight during our joint lab meetings.

Finally, I would also like to thank members of the Ackley and Lundquist lab for all their help, input, support, and friendship during my graduate school experience. I especially would like to thank my former lab mate Elvis Huarcaya Najarro for his advice and friendship throughout graduate school.

Table of Contents

Page number

List of Figures

Figure **Page number**

List of Tables

Table **Page number**

Chapter I
Introduction

The central nervous system (CNS) is composed of a myriad of intricately arranged neuronal circuits, which provide the template for the complexity that defines human behavior. Each circuit plays a pivotal role in the way humans perceive and, importantly, respond to their environment. Moreover, personality and emotions are inextricably linked to the proper wiring of the CNS. Understanding the fundamental mechanisms of the initial wiring, maintenance and modulation of the CNS is of vital importance to not only alleviating neurodevelopmental and neurodegenerative diseases associated with improper neuronal wiring, but also comprehending the human experience [1].

Underlying the innumerable circuits in the CNS exists the fundamental unit that allows for communication between the estimated 100 billion neurons in the human brain: the synapse. The inherent asymmetry of synapses allows for the continuation of nerve impulses through the specialized nature of the pre- and postsynaptic cell. The presynaptic cell contains the machinery to sense and translate action potentials at the nerve terminal into the fusion of synaptic vesicles with synaptic membrane, resulting in the release of neurotransmitters into the synaptic cleft [2]. Correspondingly, postsynaptic cells have neurotransmitter-specific receptors and intracellular machinery to relay the nerve impulse [3]. Finally, cellular adhesion molecules span the membranes of both pre- and postsynaptic cells contacting one another to first stabilize nascent synapses and then to regulate connections once they are formed [4].

On average, there are around 10^{15} synapses in the CNS, yet this number is not static; synaptic connections are formed in excess in the developing brain, only for an

existing connection to be strengthened or removed based on use or experience [5, 6]. The addition and strengthening of synaptic connections throughout an organism's lifetime is critical in the process of learning and consolidation of memories [7, 8]. In sum, proper development of neuronal circuits depends on the appropriate balance of synaptic connections established through initial formation and followed by antagonistic or agonistic manipulation of those existing connections.

The importance of synaptic modulation is accentuated in many neurological disorders, ranging from epilepsy to depression, that exhibit an imbalance in the strength and/or number [9-11]. One potential way to ameliorate these disorders would be to tip the synaptic imbalance back to its normal ratio of connections. In order to restore proper synaptic balance, it is vital to understand the mechanisms that function to restrict or assemble synaptic connections. Thus, understanding the genetic and molecular basis of synaptic modulation may provide insight into the development of pharmaceutical interventions to correct, or circumvent, synaptic imbalances found in neurological diseases.

Voltage-gated calcium channels regulate synaptic function and morphology

Research into the molecular mechanisms of synaptic biology has identified many genes required for proper synaptic function and morphology. Of these, voltage-gated calcium channels (VGCCs) have emerged as providing a critical role in neurotransmission and other aspects of synaptic biology [12]. In response to an action potential reaching the nerve terminal, VGCCs facilitate the influx of calcium

ions into presynaptic areas. This calcium influx promotes fusion of synaptic vesicles with neuronal membrane, thereby enabling the release of neurotransmitters into the synaptic cleft.

VGCCs are multimeric proteins composed of a pore forming and voltage sensing α1 subunit, along with accessory $\alpha_2\delta$, β, and γ subunits – which usually aid in channel function and localization (Fig. 1.1) [13]. The conservation of VGCC subunits allows for genetic analysis of their role in neurodevelopment to be conducted in model organisms. In *Drosophila melanogaster* and *Caenorhabditis elegans,* the α1 subunit – Cacophony and UNC-2, respectively – affects both neurotransmission and the shape of synaptic connections [14-19]. Additionally, the $\alpha_2\delta$ subunits also regulate synaptic morphology and transmission, usually by trafficking α1 subunits to the cell membrane and modulating their biophysical properties [20-22]. Interestingly, $\alpha_2\delta$ subunits have also been shown to affect synaptic morphology independent of neurotransmission [23, 24]. VGCC regulation of synaptic morphology independent of neurotransmission suggests secondary effector molecules may function downstream of channel function to shape synapses. Despite the evidence providing an understanding of how VGCCs function in neurotransmission and synaptic morphology, the molecules acting downstream of VGCCs in shaping synaptic morphology are not well understood. Identifying proteins that act in response to VGCC activation will clarify how calcium influx influences gross synaptic morphology.

VGCC-derived calcium influx, in addition to neurotransmission, initiates numerous cellular processes ranging from transcriptional regulation to cellular

death [25]. As cells must be able to translate changes in calcium concentrations into functional outputs, a wide variety of calcium-binding proteins have evolved to respond to the transient and localized nature of intracellular calcium spikes, with the most extensively studied protein being calmodulin [26].

In the nervous system, the neuronal calcium sensor (NCS) family is a diverse set of proteins that respond to fluctuations in calcium concentrations. NCS proteins possess EF hand domains, which bind calcium and induce protein conformational shifts [27]. These shifts permit NCS members to interact in a calcium-dependent manner with protein effectors. For example, in photoreceptor cells, calcium binding activates the NCS recoverin and leads to the inhibition of rhodopsin kinase [28]. Additionally, conformational rearrangements can lead to the extrusion of a membrane-targeting myristoylation sequence, allowing for a calcium-induced change in protein localization [29]. Thus, NCS proteins are attractive candidates to perform activity-independent morphological changes in response to VGCC-induced calcium influx. One of the main findings of this dissertation is the identification of an NCS protein functioning downstream of VGCCs to regulate synaptic morphology, providing the first example of such an interaction.

C. elegans GABAergic neuromuscular junction as a model for synaptogenesis

The work in this dissertation is centered on gaining insight into the molecular mechanisms of calcium signaling, and its role shaping synaptic contacts. To better understand how VGCCs and calcium-binding proteins regulate synaptic connections during development, and whether these connections are uncoupled

from neurotransmission, we utilize the model organism *C. elegans.* The nervous system of the nematode *C. elegans* functions similarly to the vertebrate CNS, but is a simplified and powerful model to study the genetics behind nervous system development [30, 31]. Adult animals possess a tractable 302 neurons, while using many of the same neurotransmitters as vertebrates. Furthermore, the connections of each neuron have all been mapped, leading it to be the first organism with a completely diagramed connectome [32].

At the synapse, the proteins involved in vertebrate synaptic transmission have orthologs in *C. elegans* [33], thus genes discovered to be involved in synaptic morphology and function can likely be used as a guide for vertebrate studies. For example, two genes originally identified in *C. elegans* for neurotransmission (by promoting synaptic vesicle fusion to plasma membrane), *unc-13* and *unc-18*, were later found to have homologues in mammals, and, fittingly, named Munc-13 and Munc18 [34, 35]. Lastly, the transparency and genetic amenability of *C. elegans* allow for *in vivo* analyses of the genes directing neurodevelopment.

Genetic analysis of synapse morphology is aided by the use of fluorescent markers to label presynaptic areas, specifically fusing the synaptic vesicle protein synaptobrevin (SNB-1) to GFP and expressing it under neuron-specific promoters. For example, the GABAergic specific promoter *unc-25* has become a widely used marker for synaptogenesis [36, 37]. This marker is observed in GABAergic neurons as punctate clusters of GFP that are evenly spaced along the ventral and dorsal nerve cord (Fig. 1.2). These puncta reliably represent NMJs, as SNB-1::GFP cluster location and incidence correspond the positions of NMJ when compared to EM

reconstructions [38]. Thus, any gene mutations that disrupt this defined SNB-1::GFP pattern are identified as regulators of synaptic morphology.

The work in this dissertation employs the *C. elegans* neuromuscular junction (NMJ) to study the genetics of synaptogenesis. Nematode NMJs contain both cholinergic (excitatory) and GABAergic (inhibitory) inputs, with these neurons innervating ventral and dorsal body wall muscles to control the animal's sinusoidal movement [39]. Postsynaptically, muscle cells extend dendrite-like arms to reach the motor neuron axons residing in the dorsal and ventral nerve cords [32]. The GABA receptor, UNC-49, clusters opposite of presynaptic areas, through instruction from an unidentified neuron derived factor [40]. In brief, the NMJ of *C. elegans* is a well-defined system recapitulating aspects of the CNS by having postsynaptic cells that receive multiple synaptic inputs from two different neuronal types (excitatory and inhibitory), thus lending itself to be a valuable resource for studying synaptogenesis.

While the NMJ consists of a tripartite system of muscle and two sets of neurons, the work in this dissertation focuses on the D-type GABAergic motor neurons. There are a total of 19 D-type GABAergic neurons, consisting of 13 VD and 6 DD neurons. Each neuron characteristically assumes a horizontal H-shape that runs the length of the animal, lying adjacent to both the dorsal and ventral body wall muscles (Fig. 1.3). While both cell bodies are located in the ventral nerve cord, VD and DD neurons differ where their presynaptic areas are positioned along the H-shape: VDs receive information in the dorsal cord and innervate the ventral body wall muscle to inhibit it, while the DDs function in the opposite manner [41]. VD and

DD synapses are formed *en passant* (i.e., along the length of the axon, instead of at the axon terminus), providing multiple synapses to occur on one neuron. In conclusion, *C. elegans* GABAergic NMJs present many advantages and opportunities to investigate the molecular mechanisms directing synaptogenesis.

Synaptic morphology dictated by a balance between adhesion and calcium signaling

The interest in VGCCs in GABAergic synapse morphology stems from a screen to identify modifiers of the synaptic phenotype that results from the loss of the extracellular matrix protein nidogen (NID-1) [14]. NID-1 is enriched in regions of the basal lamina adjacent to synaptic areas, and its absence results in elongated and abnormally shaped presynaptic areas [42]. NID-1 regulates synapses by binding the cellular adhesion molecule leukocyte-common antigen related receptor protein tyrosine phosphatase (PTP-3A) (Fig. 1.4). The effect of this interaction is to restrict synaptic vesicles and the synaptic organizing molecule SYD-2 at synapses [43]. Because the diffusion of presynaptic areas in *ptp-3A* and *nid-1* loss-of-function mutants is accompanied by the dispersal of the SYD-2 along the axonal projection, NID-1 and PTP-3 are believed to provide structural support for the maintenance of synapses. With this structural role in mind, I sought to identify the mechanism through which nidogen regulates synaptic morphology.

We found that mutations in VGCC subunits *unc-2* and *unc-36* suppressed the synaptic defects observed in nidogen mutants, and that VGCC function was required cell autonomously for regulation of synaptic morphology [14]. That this suppression

was also not dependent on synaptic transmission indicated to us VGCC activity may result in the activation of downstream effector molecules, and led to the identification of the EF hand protein CALM-1.

CALM-1 is an ortholog of the NCS protein subfamily of calcium- and integrin-binding proteins (CIB1-4), also referred to as calmyrin. CIB proteins interact with integrins to mediate platelet aggregation and adhesion [44, 45] and regulate intracellular calcium release through the inositol 1,4,5-triphosphate receptor [46]. CIB proteins also possess the ability to traffic cytoplasmic target proteins, as CIB1, in response to calcium, brings sphingosine kinase 1 via its N-terminal myristoylation sequence to the cell membrane [47].

Supporting a neural role for CIB proteins, CIB2 transcript and protein levels are enriched in the hippocampus and cortex of rats [48], and calmyrin1 interacts with microtubule destabilizing molecule stathmin2 in cultured hippocampal neurons to regulate microtubule dynamics [49]. CIB proteins are also implicated in human health, as CIB2 was identified as a risk gene in a study looking for rare copy number variants associated with autism spectrum disorders [50]. We found CALM-1 localized in the nervous system, making it an ideal candidate to serve as an intermediate between VGCCs and synaptic morphology. In fact, CALM-1 targets the *C. elegans* sphingosine kinase (SphK) to synapses in cholinergic neurons to facilitate synaptic vesicle priming [51], suggesting CALM-1 can fulfill calcium-switch properties similar to CIB proteins.

calm-1 loss-of-function mutants also suppress the enlarged synaptic areas of *nid-1* mutants, similar to VGCC subunit mutations. Double mutant analysis revealed

calm-1 and the VGCC subunits work in a linear genetic pathway, with *calm-1* functioning downstream and cell autonomously to regulate synaptic morphology. Interestingly, a gain-of-function mutation in *unc-2* mimics the synaptic phenotype of *nid-1* mutants, suggesting loss of NID-1 is similar to increased VGCC activity. These results support a model where NID-1/PTP-3 normally restrict synaptic growth by inhibiting VGCC function, and ultimately CALM-1. In conclusion, we hypothesize synaptic morphology relies a balance between VGCC-mediated calcium signaling and NID-1 regulation of synaptic adhesion.

Time-lapse analysis of GABAergic synapses, during the L4 larval developmental stage, reveals that presynaptic areas undergo marked changes in morphology, progressing from a discrete single punctum to elongated shapes (similar to *nid-1* mutant animals) that resolve into two puncta [14]. These synaptic changes require *unc-2*, as loss of UNC-2 function results in reduced dynamics. Due to the initial formation of synapses in the *unc-2* background, it is likely that UNC-2 plays a negligible role in *de novo* synapse formation. Although these data do not rule out the role of calcium signaling and synaptic adhesion at other developmental time points, it does suggest a mechanism of synapse addition from preexisting synaptic connections during organismal growth, which depends on a balance between calcium signaling and adhesion. L4 larval stage analysis contrasts with previous studies, where young adult animals were imaged, so the observed phenotypes described earlier are believed to arise from a failure to properly form synapses, rather then disassembling due to lack of stability.

In an effort to reveal potential downstream targets of VGCC/CALM-1 signaling, a calcium-dependent pulldown with CALM-1 identified the intracellular scaffolding molecule receptor for activated C kinase (RACK-1). *rack-1* loss-of-function mutants displayed synaptic defects similar to *nid-1*, indicating it also normally restricts synaptic growth. As with *nid-1* mutants, removing *calm-1* suppressed the enlarged synaptic defects of *rack-1* animals. Thus, the physical interaction between RACK-1 and CALM-1 may act as a switch between synaptic adhesion and growth.

Interestingly, the synaptic growth we observe is similar to the dynamics observed at *D. melanogaster* larval NMJs. At these NMJs, when observed from the L1 to L3 larval stage, new synaptic boutons were added by asymmetric budding or division from existing boutons [52]. Furthermore, the nascent boutons contained lower levels of the synaptic adhesion molecule FasII. These results, in combination with our *nid-1* phenotype, indicate cellular adhesion needs to be temporally down regulated to allow for the synaptic addition that accompanies organismal growth.

In summary, we have uncovered a calcium-dependent pathway that temporally regulates D-type GABAergic motor neuron synapse morphology, specifically the addition of new synapses from preexisting synaptic areas. Based on our genetic, cell biological and biochemical analyses, the addition of synaptic areas results from the expansion and budding of an existing synapse into two synaptic areas relies on the cyclical interplay between molecules responsible for synaptic stability and growth.

Section 1.1 Figures

Figure 1.1

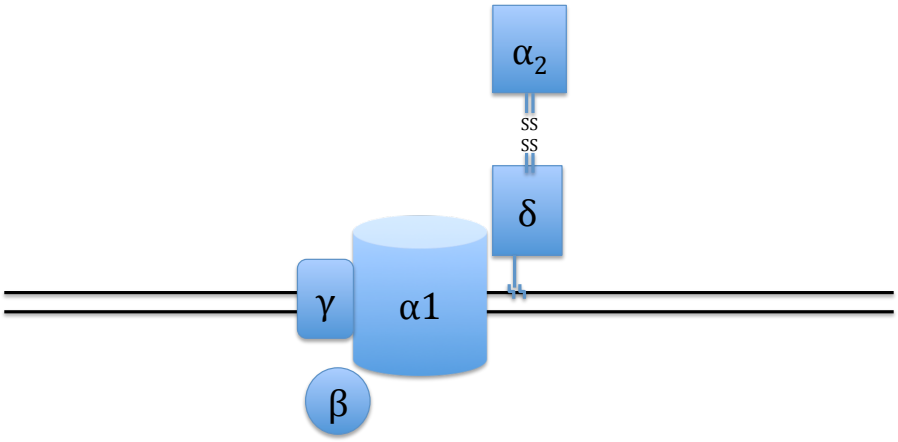

Figure 1.1 Voltage-gated calcium channels (VGCCs) are multimeric proteins VGCCs are multisubunit complexes with a principal α1-pore forming and voltage-sensing subunit. α1 subunit localization and physiological function are aided by accessory $\alpha_2\delta$, β, and occasionally γ subunits. The $\alpha_2\delta$ subunit is product of single gene that is posttranslationally cleaved into two and joined by disulfide bonds, and is believed to be tethered to the plasma membrane through a GPI anchor.

Figure 1.2

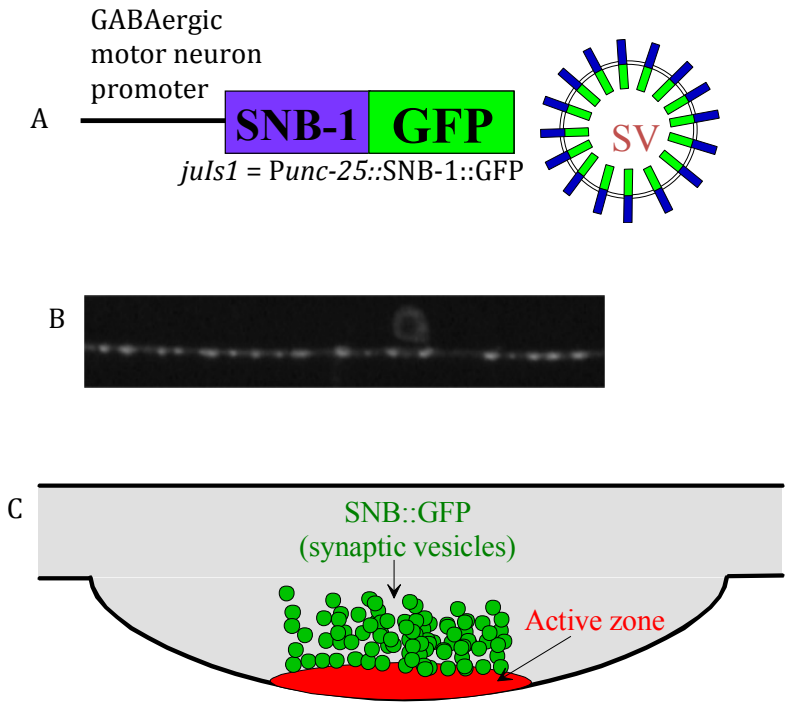
A
GABAergic
motor neuron
promoter
SNB-1
GFP
juIs1 = Punc-25::SNB-1::GFP
SV
B
C
SNB::GFP
(synaptic vesicles)
Active zone

Figure 1.2 Visualization of GABAergic NMJs (A) Synaptic areas are visualized by tagging the synaptic vesicle protein synaptobrevin with GFP. This construct is expressed under a neuron specific promoter, the GABAergic motor neuron promoter *unc-25*. (B) SNB-1::GFP puncta are observed as discrete and uniformly distributed puncta when viewed by confocal microscopy. A neuron cell body is located above the row of synaptic puncta in this image. (C) Puncta consist of an accumulation of many synaptic vesicles. Light and electron microscopy have demonstrated that puncta are collections of synaptic vesicles at single synaptic contacts.

Figure 1.3

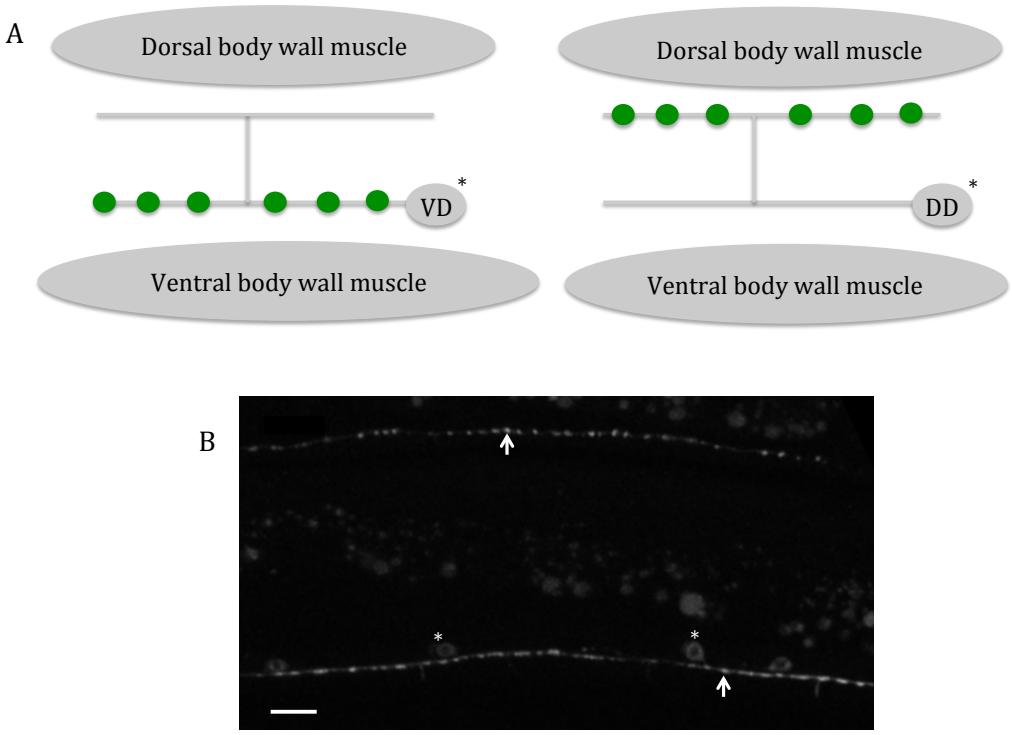
A
Dorsal body wall muscle
VD
*
Ventral body wall muscle
Dorsal body wall muscle
DD
*
Ventral body wall muscle
B
*
*

Figure 1.3 VD and DD neurons innervate ventral and dorsal body wall muscles

(A) The D-type GABAergic motor neurons consist of VD and DD neurons. These neurons form a characteristic horizontal H-shape morphology, and run along the length of the animal. Neurons have cell bodies (asterisks) along the ventral cord, with neuronal projections located in both ventral and dorsal cords, linked by a single commissure. VD and DD neurons differ by which body wall muscle they innervate. VD neurons innervate the ventral body wall muscle (indicated by green circles, representing presynaptic areas), while DD neurons innervate dorsal body wall muscles. (B) Confocal image of D-type GABAergic synapses on both ventral and dorsal cords of single animal – ventral is bottom of picture and dorsal is top of picture. Asterisks label cell bodies and arrows point to presynaptic areas. Scale bar is 10 μm.

Figure 1.4

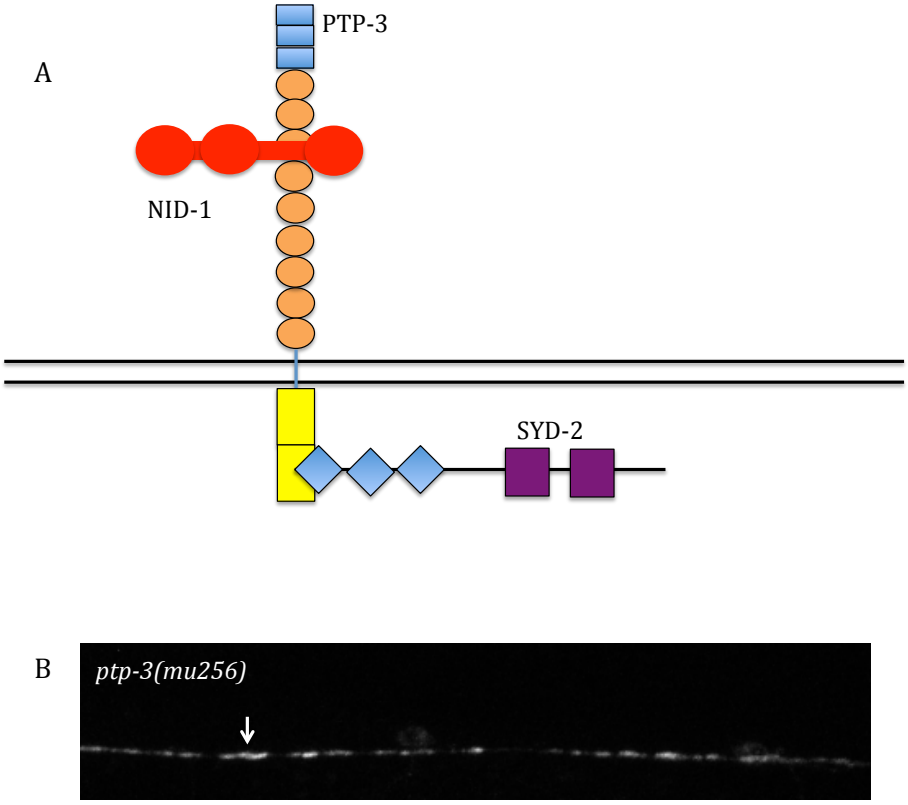

Figure 1.4 Nidogen restricts synaptic vesicles at presynaptic areas through PTP-3 (A) Nidogen interacts with transmembrane receptor tyrosine phosphatase LAR to restrict SYD-2 (liprin-α) and synaptic vesicles at the synapse. (B) Each mutation results in the same diffuse synaptic vesicle (SNB-1::GFP) accumulation, as represented by the strong loss-of-function allele *ptp-3(mu256)*. Arrow is pointed at diffuse and disorganized synaptic vesicle accumulation.

Chapter II

The *Caenorhabditis elegans* voltage-gated calcium channel subunits UNC-2 and UNC-36 and the calcium-dependent kinase UNC-43/CaMKII regulate neuromuscular junction morphology

Section 2.1 Abstract

The conserved *C. elegans* proteins NID-1/nidogen and PTP-3A/LAR-RPTP function to efficiently localize the presynaptic scaffold protein SYD-2/liprin-α at active zones. Loss of function in these molecules results in defects in the size, morphology and spacing of neuromuscular junctions.

Here we show that the Ca_v2-like voltage-gated calcium channel (VGCC) proteins, UNC-2 and UNC-36, and the Calmodulin Kinase II (CaMKII), UNC-43, function to regulate the size and morphology of presynaptic domains in *C. elegans*. *unc-2, unc-36* or *unc-43* loss-of-function mutants formed slightly larger GABAergic neuromuscular junctions (NMJs), but could suppress the synaptic morphology defects found in *nid-1/*nidogen or *ptp-3/*LAR mutants. A gain-of-function mutation in *unc-43* caused defects similar to those found in *nid-1* mutants. Mutations in *egl-19,* Ca_v1-like, or *cca-1,* Ca_v3-like, α1 subunits, or the second α2/δ subunit, *tag-180,* did not suppress *nid-1*, suggesting a specific interaction between *unc-2* and the synaptic extracellular matrix (ECM) component nidogen. Using a synaptic vesicle marker in time-lapse microscopy studies, we observed GABAergic motor neurons adding NMJ-like structures during late larval development. The synaptic bouton addition appeared to form in at least two ways: (1) *de novo* formation, where a cluster of vesicles appeared to coalesce, or (2) a single punctum became enlarged and then divided to form two discrete fluorescent puncta. Comparing to wild-type animals, we found *unc-2* mutants exhibited reduced NMJ dynamics, with fewer observed divisions during a similar stage of development.

We identified UNC-2/UNC-36 VGCCs and UNC-43/CaMKII as regulators of *C. elegans* synaptogenesis. UNC-2 has a modest role in synapse formation, but a broader role in regulating dynamic changes in the size and morphology of synapses that occur during organismal development. During the late-L4 larval stage, wild-type animals exhibit synaptic morphologies that are similar to those found in animals lacking NID-1/PTP-3 adhesion, as well as those with constitutive activation of UNC-43. Genetic evidence indicates VGCCs and the NID-1/PTP-3 adhesion complex provide opposing functions in synaptic development, suggesting that modulation of synaptic adhesion may underlie synapse development in *C. elegans.*

Section 2.2 Introduction

Changes in the cell membrane potential can open voltage-gated calcium channels (VGCC) to permit calcium entry. VGCCs are formed by α1, α2/δ, and β subunits and can include a γ subunit [53]. The α1 subunit forms the channel pore, while the auxiliary β and α2/δ subunits affect channel trafficking and physiology [54, 55]. The α2/δ subunits are synthesized as a single polypeptide that undergoes proteolytic cleavage, but remains covalently associated [56-58]. VGCCs have been classified by their pharmacological and electrophysiological properties [53]. Ca_v2-type channels are localized to the presynaptic active zone, where they function in vesicle exocytosis. Ca_v1channels localize more broadly and have been associated with events including gene regulation, local translation and dendritic growth [13].

In addition to synaptic vesicle exocytosis, there have been reports describing a role for VGCCs in regulating presynaptic development. Loss of calcium signaling through the α1 subunit *cacophony* resulted in reduced NMJ growth during Drosophila larval development [15]. At the vertebrate NMJ, a role for synaptic calcium channels has been discovered in mediating synaptic stability. The $Ca_v2.1$ and $Ca_v2.2$ calcium channels were found to bind directly to the extracellular matrix proteins laminin-10 and -11 and this interaction is critical for synaptic maintenance [59]. In the central nervous system, the α2/δ1 protein is a receptor for the extracellular matrix (ECM) protein thrombospondin, and together they act to promote synaptogenesis [24]. These results demonstrate how an interaction

between VGCCs and the synaptic ECM can regulate synaptic development and morphology.

Previously, we have shown the synaptic ECM components nidogen (*nid-1)* and collagen XVIII (*cle-1)* exhibit distinct roles in the formation of *C. elegans* NMJs [42]. Mutations in *nid-1* cause a disruption in the size, shape and function of these synapses by disrupting the accumulation of the LAR receptor tyrosine phosphatase, PTP-3A, and the intracellular-adaptor protein liprin-α/SYD-2 at active zones [43].

During a screen for *nid-1* genetic modifiers we recovered an allele of *unc-2,* which encodes the single *C. elegans* Ca_V2-like α1 subunit [17]. Loss-of-function (LOF) mutations in *unc-2* result in presynaptic contacts being slightly enlarged, but also suppression of the defects caused by the *nid-1* mutation. Using time-lapse analysis we show that GABAergic NMJs exhibit dynamic shape changes during the late L4 larval stage, and that new NMJs can be formed by the elongation and division of established presynaptic domains. These dynamic changes were dependent on functional UNC-2. We also find that *unc-43,* the *C. elegans* Calmodulin kinase II (CaMKII) homolog, regulates GABAergic synapse formation. LOF in *unc-43* suppresses *nid-1,* while a gain-of-function (GOF) mutation in *unc-43* causes *nid-1*-like defects in NMJ morphology. Our results find a novel interaction between the ECM and VGCCs, where, during synaptic development, they appear to function antagonistically.

Section 2.3 Results

unc-2 regulates the size, shape and morphology of presynaptic domains

We have found that the ECM protein nidogen, *nid-1,* affects the morphology and function of *C. elegans* NMJs [42, 43]. We visualized GABAergic NMJs using a SNB-1::GFP (synaptobrevin) chimeric marker, *juIs1* [37], as an indicator of presynaptic size and placement. In young adult (yAd) wild-type (*wt*) animals GFP-labeled synaptic vesicles cluster in discrete, regularly sized puncta that have a smooth morphology (Fig. 2.1 A), with an average area of 0.81±0.01 μm^2 (Mean±S.E.M.). Strong LOF *nid-1(cg119)* animals have a synapse defective (Syd) phenotype such that fluorescent puncta often exhibit a rough or disorganized appearance and have an apparent area of 1.45±0.08 μm^2 ($p<0.05$) (Fig. 2.1 B).

To better understand how nidogen affects NMJs, we conducted a screen for genetic modifiers of the *nid-1* phenotype (see materials and methods). We recovered *ju493*, which appeared to largely suppress the synaptic vesicle accumulation defects present in *nid-1(cg119)* animals (Fig. 2.1 C). By themselves, the *ju493* animals were uncoordinated (Unc), and also displayed synaptic morphology defects (Fig. 2.1 D). We mapped the allele to the left arm of linkage group X, and found *ju493* failed to complement *unc-2(e55)*, a strong LOF allele [17]. By PCR amplification and sequence analysis, we found that *ju493* animals had a large deletion within the *unc*-2 coding region, suggesting that it is likely a strong LOF allele (Fig. 2.1 K). *unc-2* is one of three *C. elegans* genes encoding VGCC $\alpha 1$ subunits. We tested LOF alleles in the other two VGCC, *egl-19* and *cca-1*, and did not

observe any suppression of *nid-1* defects (Sup. Fig. 2.1), indicating the observed effect is specific to *unc-2.*

We further characterized the effect of *unc-2* LOF using the *e55* allele, which causes a premature stop codon in exon 9 (Fig. 2.1 K). Presynaptic domains of *unc-2(e55)* mutants had smooth and oval-shaped SNB-1::GFP puncta, but the area of the puncta was significantly increased over *wt* by ~20% (1.04±0.07 μm^2, $p<0.05$) (Fig. 2.1 E). We also found that the total number of presynaptic clusters was slightly reduced in *unc-2(e55)* mutants (*wt* 25.6±0.2 puncta/100 μm vs. *unc-2* 22.8±0.7 puncta/100 μm ($p<0.05$)). Like *ju493*, the *e55* mutation suppressed vesicle-accumulation defects found in *nid-1(cg119)* (Fig. 2.1 F). Puncta formed in *nid-1;unc-2* double mutants had an average area of 1.15±0.10 μm^2 ($p<0.05$ vs. *nid-1* or *wt;* $p>0.05$ vs. *unc-2*), and appeared morphologically similar to *wt*.

To more quantitatively assess the NMJ morphology, we calculated the circularity of the SNB-1::GFP fluorescent puncta (Fig. 2.1 J) (see materials and methods). Wild-type SNB-1::GFP puncta are ovoid, and have an average circularity of 0.70±0.01. By comparison, in *unc-2(e55)* the puncta varied slightly, but significantly, from *wt* (0.66±0.03, $p<0.05$), while in *nid-1* mutants, the puncta were more elongated and less circular (0.60±0.01, $p<0.05$). The *nid-1;unc-2* double mutants were like *wt* (0.74±0.02, $p<0.05$ vs. *nid-1* or *unc-2;* $p>0.05$ vs. *wt*), indicating that the elongated morphology in *nid-1* was ameliorated by removing *unc-2* function.

UNC-2 is the single Ca_v2-like VGCC α1 subunit present in *C. elegans,* and is localized to the presynaptic active zone [20]. At synapses UNC-2 regulates calcium

ion entry that facilitates synaptic vesicle exocytosis [60]. It is the reduced neural transmission from motor neurons to muscles that likely results in the reduced locomotor activity and the Unc phenotype. To address that the suppression of the *nid-1* presynaptic defects was not the result of reduced exocytosis and/or locomotor activity, we tested a LOF mutation in *unc-13,* which plays essential roles in synaptic transmission and also regulates the sub-synaptic accumulation of synaptic vesicles [60, 61]. *unc-13(s69)* null mutants are also Unc, but have a more severe loss of locomotor activity than *unc-2.* In *unc-13(s69)*, puncta were slightly, but not significantly, enlarged (0.95±0.07 μm^2, $p>0.05$ vs. *wt*) (Fig. 2.1 G), and there was a significant reduction in the number of puncta formed (18.7±1.5/100 μm ($p<0.05$ vs. *wt*). In *nid-1(cg119);unc-13(s69)* double mutants, presynaptic domains were *nid-1* like, elongated and disorganized (1.29±0.10 μm^2, $p>0.05$ vs. *nid-1* and $p<0.05$ vs. *unc-13*) (Fig. 2.1 H). This result suggests that the suppression of *nid-1* by *unc-2* is unlikely to be the result of impaired exocytosis or reduced locomotion.

We identified *unc-2* as a regulator of presynaptic development because it largely suppressed the morphological defects present in *nid-1* LOF animals. Ca_V2-like channels are known to affect synaptic development [15, 59], including by linking synapses to the ECM [62, 63]. In *Drosophila* mutations in *cacophony*, a Ca_V2 $\alpha1$ voltage-gated calcium channel subunit, result in fewer NMJs being formed, although loss of syntaxin or synaptobrevin showed normal synapses, arguing the loss of the calcium channel had an effect on synapses distinct from its role in exocytosis [15]. We find that although *unc-13* mutants have fewer presynaptic domains, this effect was insufficient to suppress the morphological defects caused

by the loss of *nid-1.* It has also been shown that GABA, the neurotransmitter used by the neurons examined here, is not required for NMJ formation [36, 40]. From these results we conclude that UNC-2 regulates presynaptic development in *C. elegans* independently from neurotransmission, and the phenotype caused by the loss of NID-1 at synapses requires functional UNC-2.

Presynaptic domains exhibit developmentally dynamic morphologies

C. elegans development consists of four larval stages, ultimately leading to ~5-10-fold increase in organism length. Since no new GABAergic motor neurons are added after the first larval stage, axons of these neurons, to accommodate the increase in body size, must grow and add synapses accordingly. Since all previous observations were made in yAd animals, we examined synaptic puncta of *wt* animals in the early, mid and late L4 stages, using the maturation of the vulva as a guide for the developmental stage (Lints, in WormAtlas 2009). In the early L4 stage, SNB-1::GFP puncta in GABAergic neurons appeared of normal size (0.79±0.05 μm^2) (Fig. 2.2 A). The average area of the puncta noticeably increased starting during the mid-L4 stage (0.87±0.08 μm^2) and through the late-L4 stage (1.27±0.08 μm^2), and the puncta shapes were frequently found to be elongated, often with a disorganized perimeter (Fig. 2.2 B, C). Elongated, disorganized puncta were infrequently observed in yAd stage animals (0.81±0.01 μm^2) (Fig. 2.2 D), indicating that in *wt,* presynaptic domains have developmentally dynamic morphologies.

unc-2 mutants displayed fewer presynaptic domains than *wt* animals (Fig 2.1). We wondered if this was an effect of the failure to establish synaptic domains

during development or the deterioration of existing connections. We found that the puncta in early (0.90±0.05 μm^2) and mid L4 (0.79±0.04 μm^2) were evenly sized and regularly shaped (Fig. 2.2 E, F). However, in late L4 *unc-2(e55)* animals, enlarged puncta were observed, although to a lesser degree than *wt* (1.07±0.06 μm^2), but did not appear disorganized. Similarly sized puncta were observed in young *unc-2* adults (1.04±0.07 μm^2) (Fig. 2.2 H).

To assess the frequency of enlarged puncta relative to the total number of presynaptic domains observed, we binned individual puncta measured into categories, based on measured area (Fig. 2.3). During the late L4 stage, ~35% of the puncta in *wt* animals appeared enlarged, with an area greater than 1.4 μm^2 (~*nid-1*-like), compared to yAds, where <15% of puncta fit into that category. The increased number of enlarged puncta came at the expense of normal-sized puncta, suggesting a natural size change occurs during this period. By comparison, there was no change in the proportion of the population (26%) of puncta that measured larger than 1.4 μm^2 in *unc-2(e55)* when we compared late L4s to yAds (Fig. 2.3).

To investigate more precisely the dynamic changes in synapse morphology during the late-L4 stage, we performed time-lapse confocal microscopy on live, non-anesthetized animals (see materials and methods). In *wt* animals, we saw the following dynamic behaviors: SNB-1::GFP puncta forming *de novo,* puncta that disappeared, puncta that changed shape by increasing and decreasing in size, and at a low frequency, an existing punctum divided such that two puncta were generated (Fig. 2.4 A-C). Overall, per segment of the nerve cord examined (~150-200 μm), a net increase of 1 puncta/hour in *wt* animals was observed.

By contrast in *unc-2(e55)* animals we found little evidence of dynamic shape changes. Puncta still formed *de novo,* and puncta did enlarge, but rarely did those enlarged puncta shrink or divide (Fig. 2.4 D-F) as was seen in *wt*. Overall, per segment of the nerve cord examined *unc-2* mutants displayed a net loss of ~3 NMJ puncta/hour under our time-lapse protocol. It is not clear whether these were budding events that initiated and failed, or were delayed. The decreased number of puncta seen by GFP imaging may be due to a failure in *unc-2* animals to add and/or maintain synapses during development. Alternatively, our observations are also consistent with a significant delay in synaptic development, although not a total failure of synaptic addition. Due to the presence of *de novo* appearance of SNB-1::GFP puncta in *unc-2(e55)* mutants during the time-lapse imaging, we infer the observed synaptic dynamics likely relies on UNC-2 function after, not during, initial NMJ formation. Further, preliminary analyses indicate that synapses formed in the L3 stage of *unc-2* animals can also be enlarged, indicate the function of UNC-2 is not confined to the L4 developmental stage.

unc-36 genetically interacts with *unc-2* to regulate NMJ morphology

Mutations in *unc-36,* one of two VGCC α2/δ subunit genes in the *C. elegans* genome, often phenocopy *unc-2* [20, 64, 65], so we tested if *unc-36* was required for normal synaptic morphology. Similar to *unc-2, unc-36(e251)* caused an increase in SNB-1::GFP area in yAd animals (1.10±0.07 μm^2) ($p<0.05$) (Fig. 2.5 A). A slight, but not significant, decrease in puncta number (23.1±1.5) ($p>0.05$) was also observed. *unc-36(e251);nid-1(cg119)* double mutants appeared like *unc-36* synapses alone,

with an apparent area of 1.11±0.07 μm^2 ($p<0.05$ compared to *nid-1(cg119)* and $p>0.05$ vs. *unc-36(e251)*) (Fig. 2.5 B). Double mutants of *unc-2* and *unc-36* had puncta that resembled each of the single mutants (1.08±0.05 μm^2, $p>0.05$ vs. *unc-2* or *unc-36* alone) (Fig. 2.5 C). *unc-2(e55);unc-36(e251);nid-1(cg119)* triple mutants displayed no significant differences from either of the double mutant combinations (1.15±0.06 μm^2, $p>0.05$ vs. *unc-2;nid-1* or *unc-36;nid-1*) (Fig. 2.5 D). *unc-36* was also able to suppress *ptp-3A* defects (1.50±0.09 μm^2 ($p<0.05$) vs. *unc-36(e251);ptp-3A(ok244)* = 0.80±0.10 μm^2 ($p<0.05$)) (Fig. 2.5 E, F). From these data, we concluded *unc-2* and *unc-36* likely function in a linear genetic pathway to interact with *ptp-3A* and *nid-1* in synapse development.

We also tested the second *C. elegans* α2/δ subunit-encoding gene, *T24F1.6/tag-180* [66]. A LOF allele, *ok779,* exhibited a minor effect on SNB-1::GFP area (0.73±0.03 μm^2 ($p<0.05$)) (Sup. Fig. 2.1), and number (28.8 puncta/100 μm ($p>0.05$)) in yAd animals. *tag-180 (ok779);nid-1(cg119)* double mutants were more like *nid-1(cg119)* than the *ok779* (1.65±0.12 μm^2, $p<0.05$ vs. *nid-1* alone), indicating the suppression of *nid-1* defects is specific to *unc-36*. Double mutants of *ok779* with *unc-2* (1.02 μm^2, $p>0.05$ vs. *unc-2* alone) or *unc-36* (1.14 μm^2, $p>0.05$ vs. *unc-36* alone) similarly showed no significant change from the *unc-2* or *unc-36* single mutants.

Next we addressed whether the role of *unc-36* is cell autonomous. We were able to rescue the Unc (not shown) and Syd (Fig. 2.5 G) defects in *unc-36(e251)* by reintroducing a wild-type copy of UNC-36 under the control of the endogenous promoter (N=4 lines) (puncta area – 0.84±0.03, $p<0.05$ vs. *unc-36(e251)*). The *unc-*

36 promoter is broadly active in the animal, including the muscles and nervous system [20, 66, 67]. To determine whether *unc-36* could be functioning cell autonomously, we specifically expressed UNC-36 in the GABAergic motor neurons in *unc-36(e251);juIs1* animals. As expected, the locomotor defects were not rescued, but the size of the presynaptic puncta in these animals was significantly reduced relative to *unc-36(e251)* animals lacking the transgene (0.69±0.05, $p<0.05$ vs. *unc-36(e251)*) (Fig. 2.5 H) (N= 1 line), indicating that *unc-36* is capable of cell autonomously affecting the GABAergic NMJs.

α2/δ subunits have been implicated in synapse formation and development [22-24]. In the vertebrate central nervous system (CNS), thrombospondin (TSP) molecules act as ligands for α2/δ1. Overexpression of α2/δ1 results in increased synaptogenesis, while interfering with the TSP-α2/δ1 interaction inhibited synaptogenesis. The C-terminal region of TSP, that contains EGF repeats, binds directly to the von Willebrand factor-A domain (VWF-A) present in the α2 portion of the α2/δ1 protein [24]. Since NID-1 contains EGF repeats and localizes near NMJs [42, 68], and UNC-36 has a VWF-A domain, it is possible that NID-1 might physically interact with UNC-36. However, at GABAergic NMJs, the loss of *nid-1* causes morphological defects that are suppressed by removing *unc-36.* Also, LOF in *unc-36* has a very modest reduction in synapses formed. Thus, it seems unlikely that NID-1 acts as a ligand for UNC-36 to promote synapse addition.

There is evidence from *Drosophila* that α2/δ subunits can have effects on synaptic development independent from the α1 subunits [23]. However, our data suggest *unc-36* and *unc-2* are acting in the same genetic pathway. Work from the

Bargmann lab has demonstrated that UNC-36, along with the calcium channel chaperone CALF-1, are required for the localization of UNC-2 to the synaptic plasma membrane [20]. Thus, a simple explanation for the synaptic patterning defects would be a failure to direct UNC-2 to the synaptic plasma membrane in *unc-36(e251)* mutants. In this model, we would assume that UNC-2 is the key player required to drive changes in synaptic development, although we cannot rule out UNC-36 may have additional functions at NMJs.

unc-36 function is required during the L4 period for synaptic development

Next, to address the temporal requirement of VGCC, we used the α2/δ-antagonist Gabapentin [69] to acutely inhibit VGCC function specifically during the L4 stage of development. In cultured vertebrate neurons Gabapentin inhibits the trafficking of α2/δ subunits from the endoplasmic reticulum to the plasma membrane [70]. *wt* early L4 animals were exposed to Gabapentin (100 μM) for 24 hours. When imaged as yAds, these animals had a significant increase in SNB-1::GFP area (1.00±0.06 μm^2, $p<0.05$ vs. vehicle alone - 0.83±0.06) (Fig. 2.5 I). This suggests that Gabapentin is phenocopying *unc-36* LOF, although since presynaptic domains in double mutants of *unc-36* with *tag-180* resembled those found in *unc-36* alone, we cannot rule out that Gabapentin was broadly affecting α2/δ function.

Gabapentin treatment of *nid-1(cg119)* mutant L4 animals, resulted in a significant decrease in the SNB-1::GFP area (0.96±0.05, $p<0.05$ vs. *nid-1* alone), indicating that acute Gabapentin treatment of *nid-1(cg119)* animals during the L4 stage was able to, at least partially, suppress presynaptic defects (Fig. 2.5 J). We

conclude from our analysis that the synaptic patterning that occurs in late-L4 animals requires intact α2/δ function during that period, rather than being fixed in an earlier developmental event. *nid-1* mutants have defective presynaptic morphologies prior to L4, and these appear to be ameliorated by LOF in *unc-2.* Thus, we do not rule out a function for VGCCs prior to L4, and this result would suggest that synaptic morphologies are broadly dynamic during L4 development.

CaMKII regulates synaptic morphology

To identify molecules that might utilize changes in local calcium concentrations to shape presynaptic domains, we undertook a candidate-molecule approach. The first gene we examined was *unc-43*/CaMKII. CaMKII has been extensively linked to both pre- and postsynaptic development in multiple organisms (for review see [71, 72]). UNC-43 has been shown to work downstream of *unc*-2, and UNC-43 localization is dependent on UNC-2. CaMKII proteins have been shown to affect synapse development in multiple systems, including *C. elegans* where UNC-43 functions in the synaptic development of the glutamatergic neurons [73-75]. Because the complete loss of *unc-43* is embryonic lethal, we used a hypomorphic LOF allele, *e408. e408* yAd animals have slightly enlarged SNB-1::GFP (Fig. 2.6 A) (1.03±0.08 μm^2, $p<0.05$ vs. *wt*). Thus, reduced UNC-43 function has a similar manifestation at synapses as the loss of UNC-2 and UNC-36.

LOF in *unc-2* or *unc-36,* the *unc-43(e408)* LOF suppressed defects present in *nid-1* (Fig. 2.6 B) (1.06±0.07 μm^2, $p<0.05$ vs. *nid-1*) and *ptp-3A* yAds (*ptp-3A(ok244)* (1.03±0.12 μm^2, $p<0.05$ vs. *ptp-3A(ok244)* (1.42±0.09 μm^2)). In contrast, *unc-*

43(n498) GOF [76], bearing a constitutively activating mutation, E109K, in the active site core (numbering based on [74]), SNB-1::GFP puncta were elongated and disorganized in yAds (1.26±0.11 μm^2, $p<0.05$ vs. *wt*) (Fig. 2.6 C), and similar to *nid-1* ($p>0.05$ vs. *nid-1*).

We next examined whether *unc-43* was functioning cell autonomously by expressing an mCherry-tagged *unc-43* cDNA, under the control of the *unc-25* promoter, in the *unc-43(e408);juIs1* animals. Replacing UNC-43 specifically in the GABAergic neurons rescued the defects in *e408,* (0.83±0.05 μm^2, (N=6 lines) $p>0.05$ vs. *wt* and $p<0.05$ vs. *e408*). The RFP::UNC-43 chimera was localized throughout the cytoplasm, including being present at synapses, as evidenced by co-localization with the SNB-1::GFP (Fig. 2.6 D-G). The localization of UNC-43 suggests it could be directly functioning at NMJs to locally affect morphology.

Section 2.4 Discussion

VGCCs contribute to synaptic development in *C. elegans*

Here we show that mutations in the single Ca_V2, *unc-2,* result in changes to the number, size and shape of presynaptic domains that form during development. The overall reduction in the number of synapses formed in *unc-2* mutants is modest, suggesting that the primary role of VGCCs is not to promote *de novo* synapse addition. Rather, UNC-2 function is most evident in the maintenance of presynaptic domain morphology, as *unc-2* mutants display areas that are enlarged relative to wild type.

The function of *unc-2* in regulating presynaptic morphology is also observed when the synaptically associated adhesion molecules NID-1 or PTP-3A are absent. Removing UNC-2 from *nid-1* or *ptp-3* loss-of-function backgrounds ameliorates the mislocalization of presynaptic proteins and synaptic overgrowth in those mutants. This indicates that the morphological changes associated with the loss of NID-1-mediated adhesion require functional UNC-2, but independent of synaptic vesicle exocytosis.

Regulation of adhesion and growth at synapses

Synapses are dynamic structures that can be added or removed, or change shape to accommodate functional changes in neural networks and/or organismal growth. In Drosophila, transient changes in adhesion have been shown directly to permit switching between synaptic stability and synaptic growth [52, 77-81]. Molecularly, both Fas2 and *discs large* (DLG) appear to be important for synaptic

stability. Down regulation of Fas2-mediated adhesion by activation of CaMKII has been shown to specifically induce synaptic growth [79-81].

DLAR, the Drosophila PTP-3 homolog, has also been shown to complex with different ligands to switch between synaptic stability and synaptic growth [78]. In vertebrates, cell adhesion molecules like laminins and nidogens are required for NMJ maintenance. In cultured vertebrate neurons, regulation of liprin-α, via CaMKII, has been shown to regulate LAR to affect dendritic spine stability at excitatory synapses [79]. Overall, these findings suggest that changes in synaptic morphology that occur normally in development require modulation of the synaptic adhesion that maintains synaptic structure.

Using time-lapse analysis we find that, in *C. elegans,* during a specific developmental window, presynaptic domains in wild-type animals can be morphologically similar to those found in *nid-1/ptp-3A* mutant adults. Further, we observed that a *nid-1*-like elongated punctum could divide to form multiple new puncta. These dynamics, both elongation and division, were dependent on *unc-2.* Based on our results and data from other systems, a simple model is that nidogen-LAR adhesion maintains NMJ structure, and that developmental changes in synaptic morphology require transient inhibition of nidogen-LAR adhesion, and that this occurs via a pathway that includes UNC-2, UNC-36 and UNC-43.

Cooperative vs. antagonistic interactions between the ECM and VGCCs in synaptic maintenance

Previous work has shown that the ECM and the VGCCs work cooperatively to stimulate synapse development [24, 59, 63]. For example, the synaptically associated laminin β2 subunit can directly bind to an extracellular loop in the VGCC α1 polypeptide. In cultured neurons, this interaction induces the clustering of synaptic vesicles at the binding site. However, neither the genetic ablation of either $Ca_v2.1$ or laminin β2, nor disrupting the binding of these proteins *in vivo* results in a total failure in synapse formation [59]. Rather, a defect in synaptic growth and/or maintenance was observed in those animals. Similarly, NMJs in mice lacking nidogen-2 do form normally, but fail to develop, beginning to fragment around three weeks after birth, suggesting a role in synaptic maintenance for nidogen-2 as well [82], although no interaction has been described between nidogen and VGCCs in vertebrates.

We have found that nidogen is required for synaptic maintenance, which suggests a conservation of function for this ECM molecule. However, we also see that the defects observed in *nid-1* mutants require functional UNC-2 VGCCs. Thus, in contrast to the apparent cooperative interaction observed in vertebrates, our study suggests perhaps an antagonistic interaction between VGCCs and ECMs in *C. elegans*. It is possible that our findings reflect a difference in the growth of vertebrate NMJs that form at axon terminals and *C. elegans* NMJs that form *en passant*.

It is worth noting that we also find that presynaptic domains in *unc-2* mutants are slightly enlarged, compared to wild-type animals. This may seem

contradictory in that the loss of *unc-2* also limits synapses from elongating during specific periods of development or when *nid-1* is absent. A simple way of thinking about this is that in the absence of UNC-2, NMJs are too stable, unable to respond to signals that instruct them to enlarge or shrink. This would be a novel finding for this class of VGCCs; that they function as key regulators of dynamic changes in synaptic morphology. Going forward our goal will be to identify how UNC-2 can regulate these seemingly distinct functions at NMJs.

Section 2.5 Materials and Methods

C. elegans strains

All *C. elegans* strains were maintained at 20-22.5 ºC as described [83]. The following alleles were used in this report: N2 (var. Bristol), *nid-1(cg119), unc-2(ju493), unc-2(e55), unc-36(e251), tag-180(ok779), egl-19(n582), cca-1(ad1650), ptp-3A(tm352)*, *ptp-3A(ok244), ptp-3(mu256), unc-43(n498), unc-43(e408), rpm-1(ju44), unc-13(s69), tra-2(q276)/mnC1*. The following integrated strain was used: *juIs1* [*Punc-25::*SNB-1::GFP]. Transgenic animals were generated by germ line transformation as described [84]. To conduct the *ju493/e55* non-complementation, *tra-2(q276); juIs1/+;ju493/+* XX males were crossed to *unc-2(e55)* hermaphrodites. Cross progeny were identified by presence of GFP (*juIs1*), non-complementation was determined by presence of UncGfp animals.

Genetic Modifier Screen

nid-1(cg119);rpm-1(ju44);juIs1 animals were mutagenized using 50mM ethane methyl sulfonate (EMS). F2 animals were scored for a hypercontracted uncoordinated phenotype that is observed in *syd-2;rpm-1* double mutants. Individual HypUnc animals were allowed to self-fertilize to insure transmission of the phenotype. The animals were outcrossed to either *nid-1(cg119)* or *rpm-1(ju44)* single mutant backgrounds to determine the effect of new mutations. (Genetic modifier screen conducted by Dr. Brian Ackley.)

Image Analysis

Synapse morphology of D-type neurons was visualized by juIs1 [Punc-25 SNB-1::GFP]. All images were collected on either a Zeiss Pascal confocal microscope or an Olympus FV1000 confocal microscope equipped with Fluoview software. Images were acquired using multi-track parameters when necessary (unc-36 and unc-43 rescue), with either a 63X or 60X Plan-apochromat objective, respectively. Animals were anesthetized using 0.5% phenoxy-propanol (TCI America) in M9 and mounted on 2% agarose pads. Measurements of SNB-1::GFP were as described with minor modifications [42]. All images were collected using the exact same microscope settings. Briefly, confocal images were projected into a single plane using the maximum projection and exported as a tiff file with a scale bar. Using ImageJ the files were converted to a binary image using the threshold command, so that the binary image resembled the RGB image. A region of interest was drawn around the relevant region of the nerve cords. The following measurement options were selected: Area, Center of Mass, Circularity, Perimeter, Fit Ellipse, and Limit to Threshold. Scaling was set by measuring the scale bar. The "Analyze Particle" command was used with a minimum of four pixels and no maximum size. The following options were selected: Outline Particles, Ignore Particles Touching Edge, Include Interior Holes and Reset Counter. The resulting measurements were exported to Microsoft Excel and GraphPad Prism for statistical analysis. Comparisons of single mutants to the wild-type were tested by Students two-tailed t-test, while double and triple mutant combinations were compared within the

group using a Kruskal-Wallis test with a Dunn's Multiple Comparison post hoc test. Circularity is a measure of how close to a perfect circle an object is, where 0 is a line and 1 is a perfect circle. The test relates the area of the observed object to the area of a circle with the same radius (formula = 4pi*(area/perimeter^2)).

UNC-36 rescue

To rescue the *unc-36(e251)* defect we generated a PCR product including the putative promoter and endogenous 3'UTR using the following primers (*unc-36promF1: 5'-ccacgtacatagaattcggaatc-3'* and *unc-36 3'UTR R1: 5'-caaggcagttggaaagtcgac-3'*). The PCR product was TOPO cloned into pCRXLII (Life Technologies) to generate pBA234. pBA234 was injected at 10 ng/μl into *unc-36(e251);juIs1* animals along with pPD118.33 (*Pmyo-2::gfp*) as a co-injection marker, plus pBA186 (*Punc-25::mCherry)* to mark the GABAergic motor neurons containing the transgene.

Cell-specific rescue

A genomic fragment covering the *unc-36* coding region was amplified using the following primers (*unc-36promF1: 5'-ccacgtacatagaattcggaatc-3'* and *unc-36 3'UTR R1: 5'- caaggcagttggaaagtcgac-3'*). The PCR product was T/A cloned into the pCR8/GW/TOPO vector (Life Technologies), and then was recombined using L/R clonase (Life Technologies) into pBA153, creating pEVL404 (*Punc-25::unc-36).* (Undergraduate Gavin Hanson made this construct for analysis.) pEVL404 was injected into *unc-36(e251);juIs1* animals at 10 ng/μl along with pPD118.33 (*Pmyo-*

2::gfp) as a co-injection marker. For *unc-43,* we isolated a full-length cDNA for UNC-43D isoform by RT-PCR from wild-type RNA isolated by Trizol using the following primers (*unc-43cDNA F1: 5'-atgatgaacgcaagcacca-3'* and *unc-43cDNA R1: 5'-ctagaattcagatactgttgtatttgttg-3'*). (RNA isolation done by Dr. Brian Ackley.) Using the InFusion (Clontech) enzyme this product was recombined into pEVL387 (*Punc-25::mCherry::unc-43 3' UTR*) to generate pEVL400 (*Punc-25::mCherry::unc-43E::unc-43 3'UTR*). The pEVL400 plasmid was injected into *unc-43(e408);juIs1* at 5 ng/μl. Any additional information about sequences or cloning procedures is available upon request.

Time-lapse analysis

L4 animals were immobilized on 10% agarose pads in the presence of 5% (w/v) polystyrene beads (Bangs Laboratory). Animals were imaged at 5-minute intervals for 1 hour. Animals that died during the acquisition process (as determined by a rapid and dramatic increase in intestinal autofluorescence) were excluded from the analysis. Images were then exported to ImageJ. Z-stacks were produced for each time point, and then times 0 and 60 minutes were thresholded, converted to masks and overlaid as false colored, green and red respectively. This allowed simple determination of spots that were added or removed, grew or shrank or divided during the analysis period. The total number of puncta added/lost during the hour session was determined by comparing initial time and final time points for the appearance or disappearance of puncta.

Pharmacology

Gabapentin (Sigma Aldrich) was resuspended in DMSO at 100 mM, and then diluted in 1:10 in PBS and added to standard NGM plates seeded with OP50 *E. coli* to achieve the final desired concentration. Using plates with an increasing dose of Gabapentin, we found that animals reared throughout development on NGM plates containing 100 μM Gabapentin phenotypically resembled *unc-36,* appearing thin, with poor movement (data not shown), thus we used this concentration for our experiments. Plates were permitted to dry overnight and then 20 L4 animals of each genotype were placed on the media. Animals were imaged 24 hours later (as young adults). (Experiment conducted by Dr. Brian Ackley.)

Section 2.6 Figures

Figure 2.1

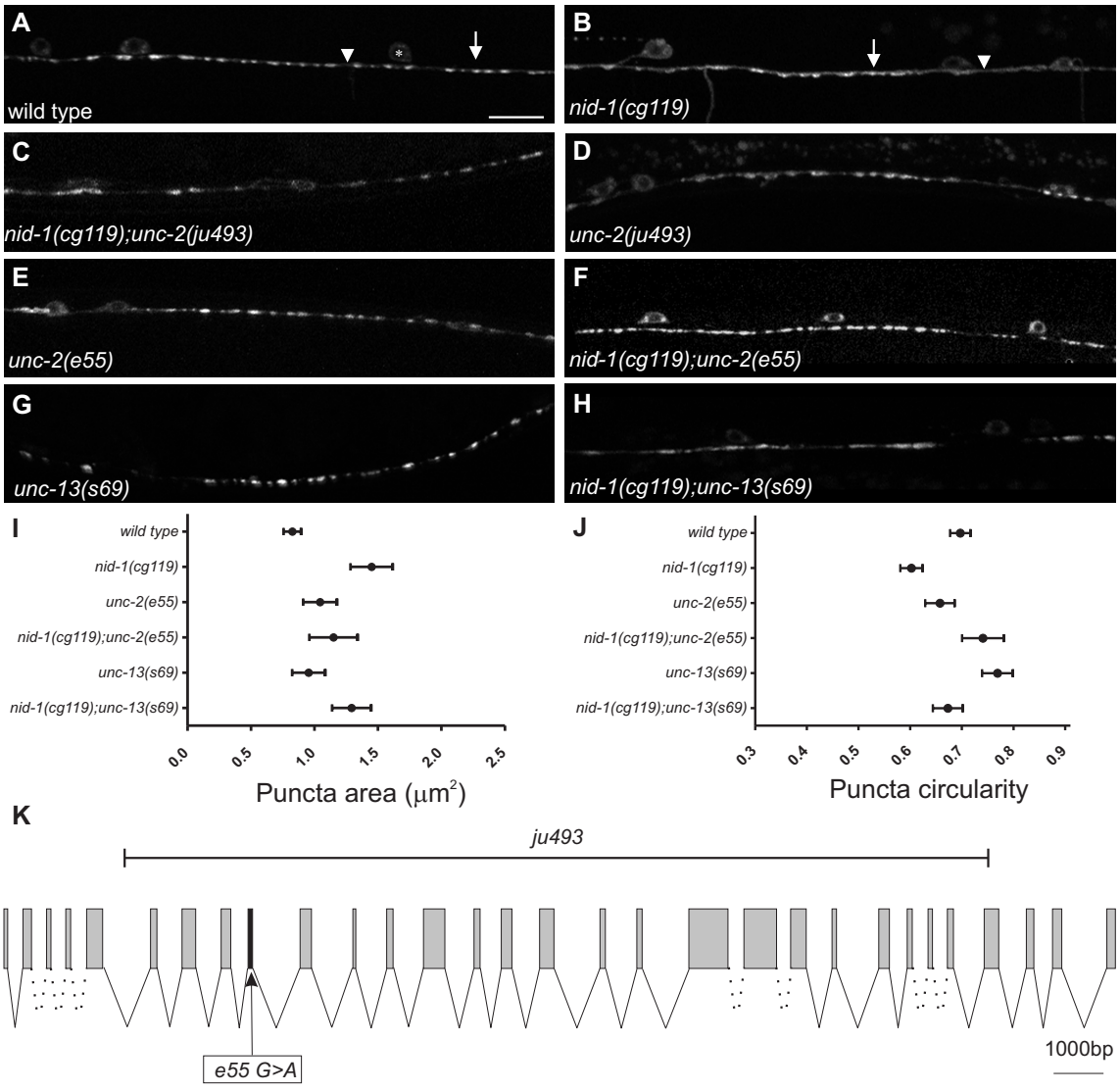

Figure 2.1 *unc-2* mutations suppress SNB-1::GFP defects in *nid-1* (A) In wild-type animals synaptic vesicles accumulated in puncta (arrow) that have smooth morphology and are evenly spaced (arrowhead). Cell bodies (asterisks) are also visible. Scale bar is equivalent to 10 μm. (B) Animals lacking nidogen accumulated synaptic vesicles in elongated (arrow) puncta. Diffuse GFP was often present in the regions between puncta (arrowhead). (C) The *ju493* mutation suppressed the large aggregations of SNB-1::GFP seen in *nid-1* mutants. (D, E) Mutations in *unc-2* (D – *ju493*, E – *e55*) resulted in slightly larger puncta, but the morphology and distribution were more similar to wild type, than *nid-1*, even when *nid-1* was absent (F). (G) *unc-13(s69)* animals had a slight decrease in the number of puncta formed, but the morphology was not grossly affected. (H) In the *nid-1(cg119);unc-13(s69)* double mutants puncta were elongated similar to *nid-1* single mutants. (I, J) We quantified the puncta area (K) and circularity (L) for each of the analyzed genotypes and plotted them as mean (circle) with the 5-95% confidence interval (whiskers). (K) A cartoon of the genomic region of *unc-2* with the position of alleles used indicated. Exon/introns are to scale, except for dashed lines, which indicate larger introns. The *e55* allele is a G>A nucleotide change in exon 9 that results in Q571 to stop (numbering for UNC-2 isoform E). The *ju493* deletion removes a large part of the coding segment, corresponding to the exons encoding AA144-1888. All animals in these micrographs are young adults (1-2 days post L4). (Image acquisition and analysis conducted by Dr. Brian Ackley.)

Figure 2.2

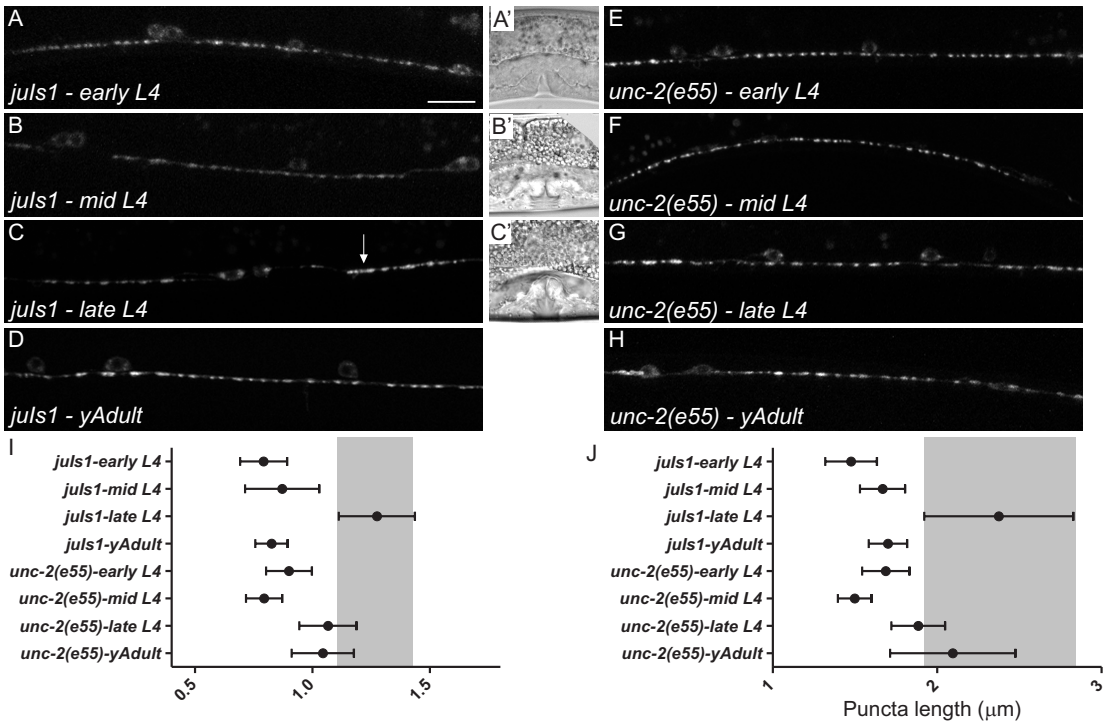
A
juIs1 - early L4
A'
E
unc-2(e55) - early L4
B
juIs1 - mid L4
B'
F
unc-2(e55) - mid L4
C
juIs1 - late L4
C'
G
unc-2(e55) - late L4
D
juIs1 - yAdult
H
unc-2(e55) - yAdult
I
juIs1-early L4
juIs1-mid L4
juIs1-late L4
juIs1-yAdult
unc-2(e55)-early L4
unc-2(e55)-mid L4
unc-2(e55)-late L4
unc-2(e55)-yAdult
0.5
1.0
1.5
J
juIs1-early L4
juIs1-mid L4
juIs1-late L4
juIs1-yAdult
unc-2(e55)-early L4
unc-2(e55)-mid L4
unc-2(e55)-late L4
unc-2(e55)-yAdult
1
2
3
Puncta length (μm)

Figure 2.2 wt animals have enlarged puncta during late L4 development During the early (A) and mid (B) L4 stage SNB-1::GFP puncta in wild type animals were evenly sized and spaced. (C) But during late L4 puncta were often enlarged and/or elongated (arrow) along the axon. (A'-C') Representative examples of vulval progression used to mark transition from early (A'), mid (B') and late (C') phases of L4 development. (D) In young adults puncta were again evenly sized and spaced. In *unc-2* mutants the early (E) and mid (F) L4 stage animals had evenly sized and spaced puncta, that appeared enlarged in late L4 (G), but not elongated. (H) Puncta remained enlarged in young *e55* adults, compared to those in equivalently aged wild-type animals (D). (I) Plots of the puncta length in the different stages are presented as means (circles) with the 5-95% confidence intervals (whiskers). During late L4 of wild type (area also shaded for comparison), puncta are longer, and more variable in length, than during other periods imaged. By comparison, during late L4, although longer than wild type adults, *unc-2* mutants had only a modest increase in length. (J) A plot of the length of each puncta divided by the width for each genotype.

Figure 2.3

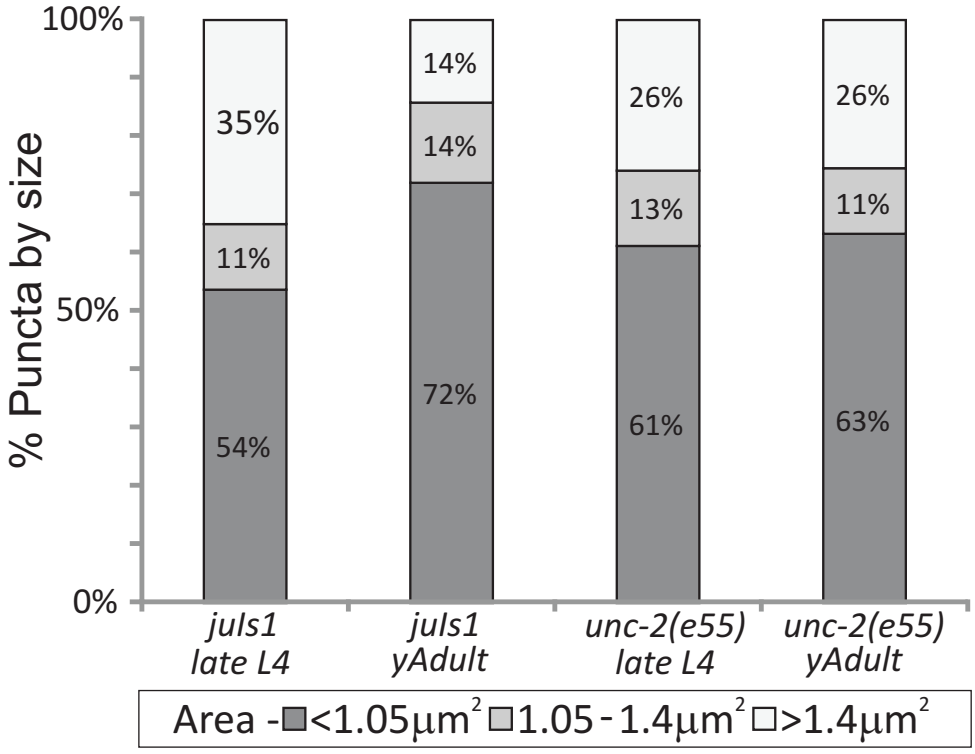
100%
50%
0%
% Puncta by size
35%
11%
54%
14%
14%
72%
26%
13%
61%
26%
11%
63%
juls1 late L4
juls1 yAdult
unc-2(e55) late L4
unc-2(e55) yAdult
Area - <1.05μm² 1.05 - 1.4μm² >1.4μm²

Figure 2.3 Presynaptic domains reshape during L4 to adult transition The proportion of puncta with an enlarged shape was analyzed. Puncta were binned into three categories based on the area [(<1.05, wild-type like), (1.05-1.40, *unc-2* like) and (>1.40, *nid-1* like)]. During late L4 in wild type 35% of the puncta were enlarged and appeared *nid-1* like, compared to only 14% in young adults. In contrast, the percent of puncta in *unc-2* animals in any of the categories was not changed during the L4 developmental stage. N>150 puncta/genotype/stage.

Figure 2.4

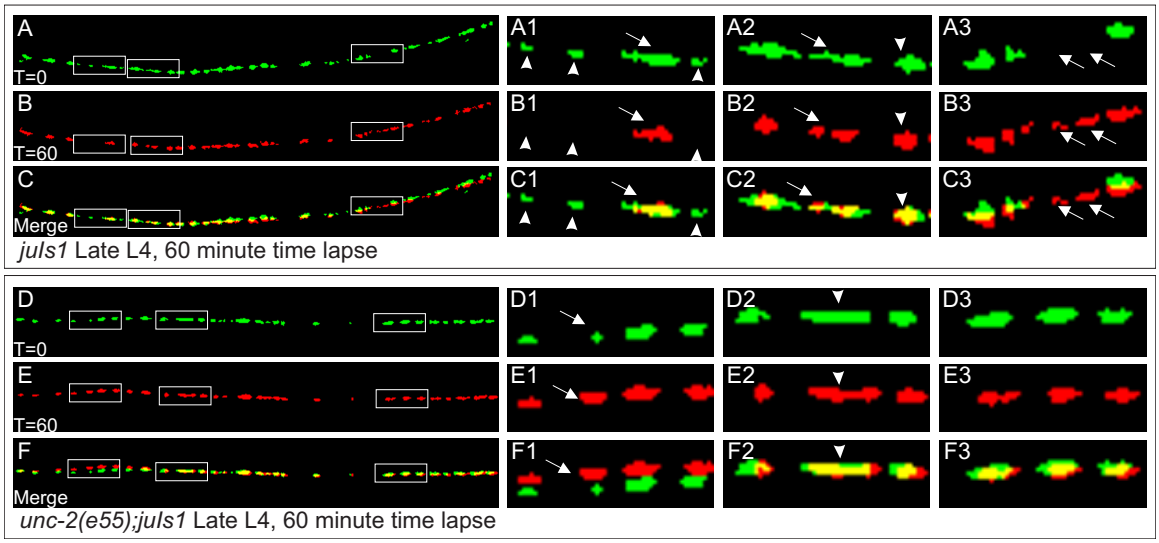
A
T=0
A1
A2
A3
B
T=60
B1
B2
B3
C
Merge
C1
C2
C3
juIs1 Late L4, 60 minute time lapse
D
T=0
D1
D2
D3
E
T=60
E1
E2
E3
F
Merge
F1
F2
F3
unc-2(e55);juIs1 Late L4, 60 minute time lapse

Figure 2.4 *unc-2* mutants exhibit fewer dynamic NMJs during the L4 stage SNB-1::GFP puncta formed in the ventral cord of wild-type or *unc-2(e55)* animals were imaged for one hour. The panels are a mask of the threshold image and false colored each to demonstrate changes in the shape of the puncta. In wild type after one hour the puncta largely align (yellow), with some differences, highlighted in the boxed regions. (A-C1) Three small puncta (arrowheads) that are present at time 0 have disappeared 60 minutes later (B1). The elongated puncta (arrow) has condensed. (A-C2) An elongated punctum present at time 0 (arrow) appears to have separated into two distinct puncta by the end of the observation period. An adjacent punctum (arrowhead) is largely unchanged over the time period. (A-C3) There is an empty space at time 0 in which has two puncta (arrows) have formed by the time 60 point. (D-F) In *unc-2* mutants puncta generally enlarged, but we observed fewer formation/elimination and division events. (D-F1) One punctum (arrow) was approximately twice as large after 60 minutes, while the adjacent puncta were largely unchanged. Note: the animal moved slightly during the protocol, putting the puncta in D1-F1 slightly out of alignment. (D-F2) In some instances we found puncta that appeared to be elongated (arrowhead). In *unc-2* these elongated puncta remained elongated after an hour whereas in wild-type they often resolved into two puncta, or shrunk over the imaging period (A-C2). (D-F3) Many of the SNB-1::GFP puncta were approximately the same size, undergoing little change during the time lapse, indicating that photobleaching was not grossly affecting the SNB-1::GFP over the imaging protocol.

Figure 2.5

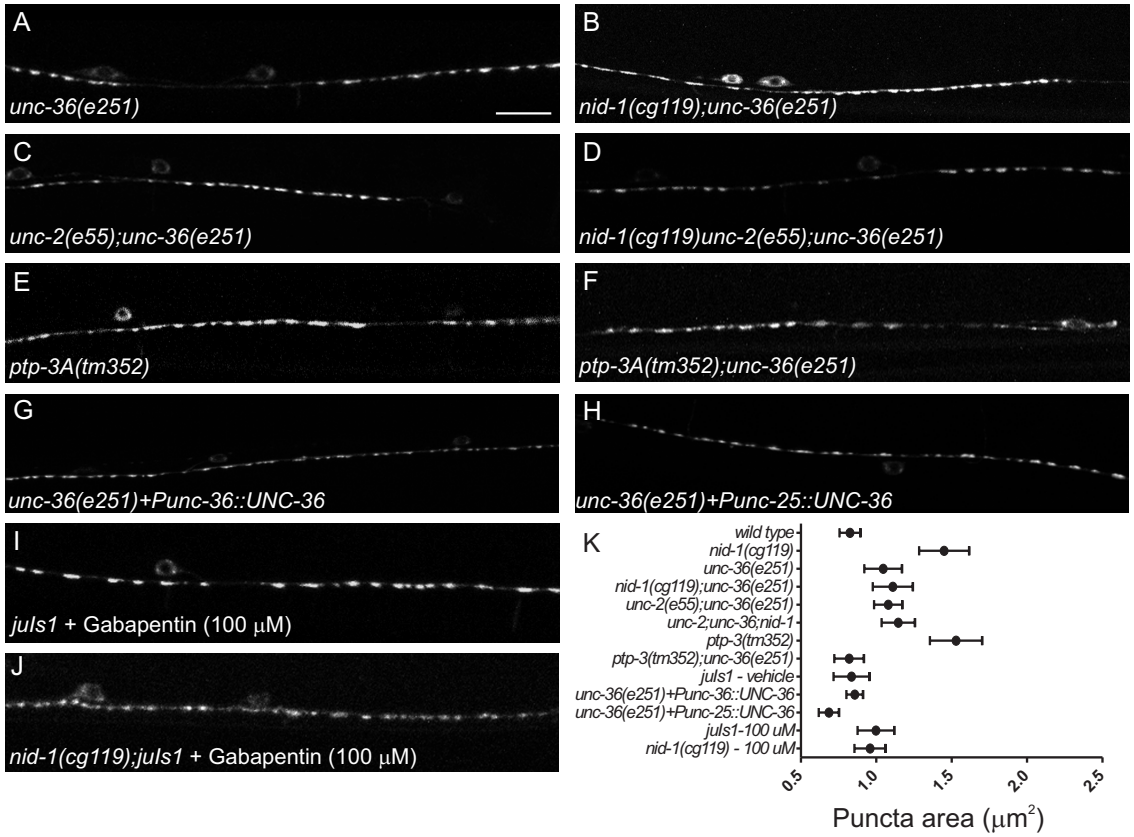
A
unc-36(e251)
B
nid-1(cg119);unc-36(e251)
C
unc-2(e55);unc-36(e251)
D
nid-1(cg119)unc-2(e55);unc-36(e251)
E
ptp-3A(tm352)
F
ptp-3A(tm352);unc-36(e251)
G
unc-36(e251)+Punc-36::UNC-36
H
unc-36(e251)+Punc-25::UNC-36
I
juIs1 + Gabapentin (100 μM)
J
nid-1(cg119);juIs1 + Gabapentin (100 μM)
K
wild type
nid-1(cg119)
unc-36(e251)
nid-1(cg119);unc-36(e251)
unc-2(e55);unc-36(e251)
unc-2;unc-36;nid-1
ptp-3(tm352)
ptp-3(tm352);unc-36(e251)
juIs1 - vehicle
unc-36(e251)+Punc-36::UNC-36
unc-36(e251)+Punc-25::UNC-36
juIs1-100 uM
nid-1(cg119) - 100 uM
0.5
1.0
1.5
2.0
2.5
Puncta area (μm²)

Figure 2.5 *unc-36* regulates presynaptic morphology (A, B) *unc-36* mutants also had slightly enlarged puncta, and also suppressed the defects in *nid-1.* (C) *unc-2;unc-36* mutants appeared similar to the single mutants, but were not further enlarged. (D) Suppression of *nid-1* was not enhanced by simultaneous loss of both *unc-2* and *unc-36.* (E) A deletion in the *ptp-3A* specific coding region, *tm352,* causes a *nid-1* like defect in synapses, which is also suppressed by loss of *unc-36* (F). (G) Broadly replacing UNC-36 function via transgene efficiently rescued the enlarged puncta found in *unc-36(e251)* mutants. (H) Specific expression of UNC-36 solely in the D-type motor neurons was also sufficient to reduce the puncta enlargement found in *unc-36(e251)*. (I, J) Treatment of wild-type animals (I) or *nid-1(cg119)* (J) with the α2/δ-subunit antagonist, Gabapentin, resulted in enlarged puncta similar to those found in *e251.* (K) The puncta area by genotype are plotted as the mean (circle) with 5-95% confidence interval (whiskers). All animals in these micrographs are young adults (1-2 days post L4). (Image acquisition and analysis, with the exception of panels C and D, conducted by Dr. Brian Ackley.)

Figure 2.6

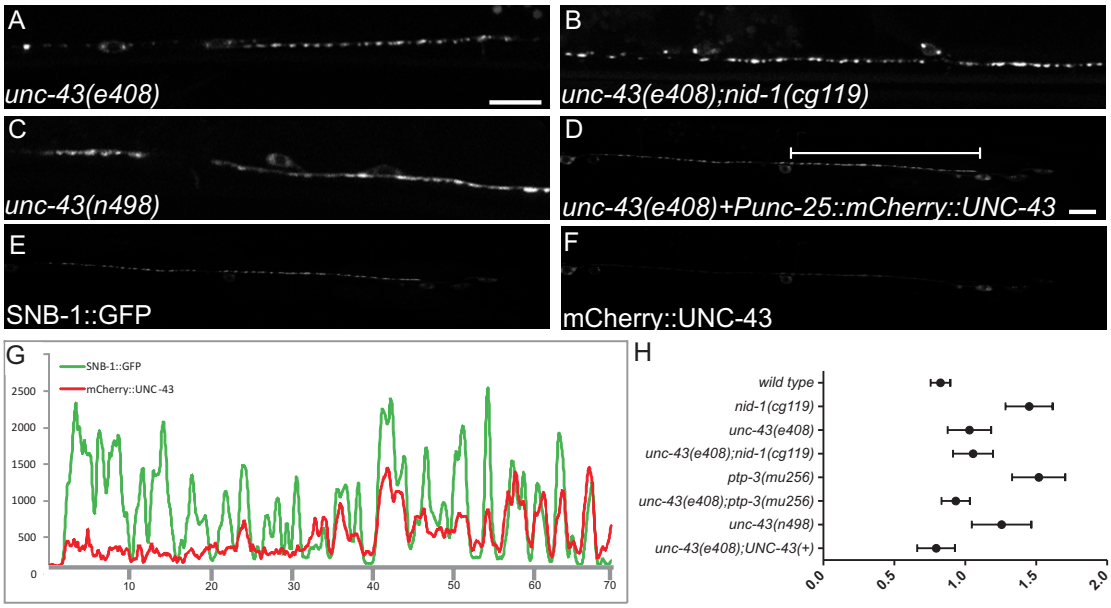
A
unc-43(e408)
B
unc-43(e408);nid-1(cg119)
C
unc-43(n498)
D
unc-43(e408)+Punc-25::mCherry::UNC-43
E
SNB-1::GFP
F
mCherry::UNC-43
G
SNB-1::GFP
mCherry::UNC-43
2500
2000
1500
1000
500
0
10
20
30
40
50
60
70
H
wild type
nid-1(cg119)
unc-43(e408)
unc-43(e408);nid-1(cg119)
ptp-3(mu256)
unc-43(e408);ptp-3(mu256)
unc-43(n498)
unc-43(e408);UNC-43(+)
0.0
0.5
1.0
1.5
2.0

Figure 2.6 *unc-43* can cell autonomously regulate presynaptic morphology (A) The *unc-43(e408)* LOF mutation caused an increase in puncta size. (B) The *e408* mutation suppressed the morphological defects found in the *nid-1* background. (C) The *n498* GOF mutation in *unc-43* caused enlarged puncta that were disorganized. (D-F) Expression of an mCherry-tagged UNC-43 chimera specifically in the GABAergic neurons largely rescued the SNB-1::GFP morphology defects present in *e408* animals. (G) A line scan of the VD12 axon region (line in panel D) demonstrating the co-incidence of mCherry::UNC-43 (red) with SNB-1::GFP (green). GFP/RFP coincidence was measured in a single confocal slice. (H) A plot of the puncta area measured by genotype as mean (circle) with the 5-95% confidence interval (whiskers). All animals in these micrographs are young adults (1-2 days post L4).

Supplementary Figure 2.1

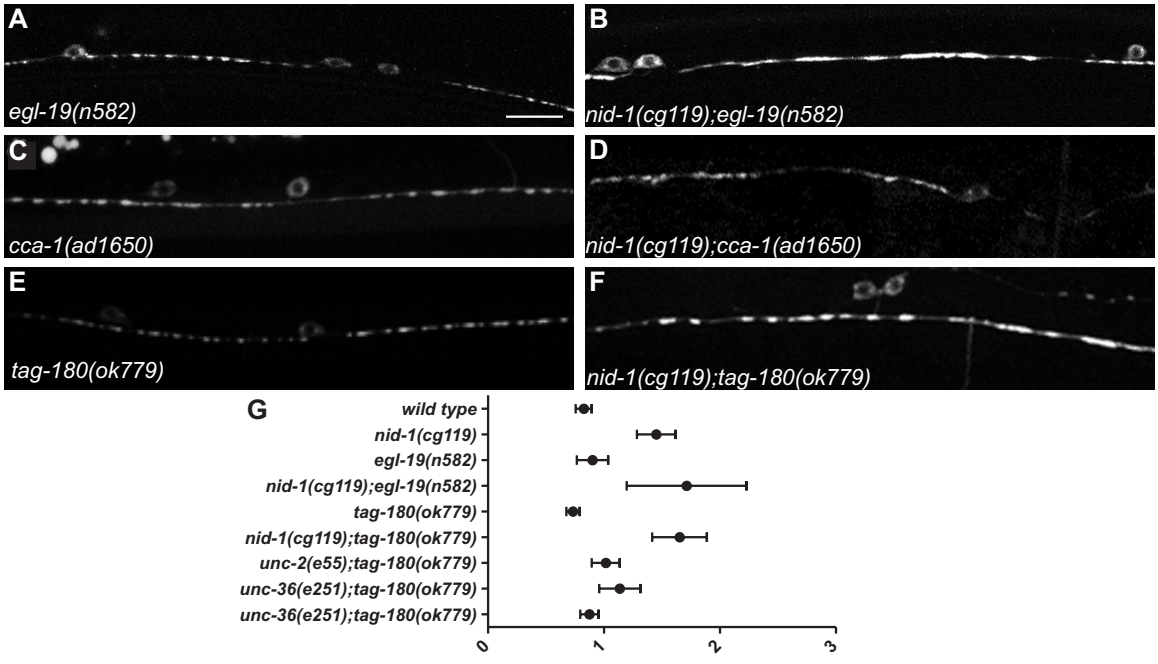

Supplemental Figure 2.1 Specificity of interaction between *unc-2/unc-36* and *nid-1* (A) The *egl-19* LOF allele, *n582,* animals had normal appearing SNB-1::GFP puncta. (B) In *egl-19(n582);nid-1(cg119)* the puncta appear enlarged and disorganized. (C) A deletion in the Cav3-like channel, *cca-1,* had no obvious effect on SNB-1::GFP morphology. (D) Removing *cca-1* from *nid-1* mutants did not suppress the morphological changes, as puncta were observed to be elongated and disorganized. (E) Loss of the second $\alpha 2/\delta$ subunit, *tag-180,* had only a modest effect on SNB-1::GFP puncta, but did not suppress the defects found in *nid-1* mutants (F). (G) A plot of the puncta area measured by genotype as mean (circle) with the 5-95% confidence interval (whiskers). All animals in these micrographs are young adults (1-2 days post L4). (Image acquisition and analysis of panels A-D conducted by Dr. Brian Ackley.)

Chapter III

CALM-1, the *Caenorhabditis elegans* calmyrin ortholog, functions with the voltage-gated calcium channels UNC-2 and UNC-36 to regulate neuromuscular junction morphology

Section 3.1 Abstract

Synapses are intercellular junctions that facilitate communication between a neuron and its target. Once formed, synapses undergo regulated changes in size, shape and activity to strengthen, or remove, existing connections. Previously, we have shown the *Caenorhabditis elegans* voltage-gated calcium channel subunits UNC-2 and UNC-36 mediate changes in GABAergic neuromuscular junctions (NMJs) that occur concurrently with organismal growth. In this study, we show that a gain-of-function mutation in *unc-2* caused synaptic overgrowth, resulting in a phenotype resembling the loss of extracellular matrix molecule nidogen. Both *unc-2* gain-of-function and *nid-1* loss-of-function phenotypes were suppressed by loss of function in *calm-1,* the single *C. elegans* ortholog of the calcium- and integrin-binding protein (CIB), additionally known as calmyrin. Expression of *calm-1* in the GABAergic motor neurons was able to rescue the synaptic phenotype, indicating *calm-1* can function cell autonomously. We found CALM-1 binds to the adaptor protein RACK-1 in a calcium-dependent manner. Loss of *rack-1* function causes a *nid-1*-like phenotype at GABAergic NMJs, and this phenotype could be suppressed by removing *calm-1.* We conclude CALM-1 functions cell autonomously and downstream of UNC-2/UNC-36 to regulate synapse morphology.

Section 3.2 Introduction

Voltage-gated calcium channels (VGCCs) are multimeric proteins that facilitate neurotransmitter release in response to nerve terminal membrane depolarization. Structurally, VGCCs are composed of a voltage sensing and pore forming α1 subunit assembled with β, α2/δ and, occasionally, γ auxiliary subunits, which regulate channel localization and biophysical properties [85]. VGCC α1 subunit function is conserved through evolution, as its loss in *Caenorhabditis elegans* results in decreased neurotransmitter release [17, 18, 60] and in *Drosophila*, where α1 subunit mutants also decrease neuronal firing [19].

VGCCs also regulate synaptic morphology, and this regulation has been found to occur independent of neuronal activity in both *C. elegans* and *Drosophila* [14, 15, 23]. Moreover, in the vertebrate central nervous system, thrombospondin receptor α2δ-1 can promote synaptogenesis in the presence of drugs that block calcium channel function [24]. These findings indicate VGCCs can provide an activity-independent signal to shape synaptic morphology.

VGCC-derived calcium influx, in addition to neurotransmission, can initiate a myriad of cellular processes, encompassing events ranging from transcriptional regulation to cellular death [25]. With the ability to translate ionic concentrations into functional outputs, the neuronal calcium sensor (NCS) family is a diverse set of proteins that have evolved to respond to the transient and localized nature of intracellular calcium spikes. NCS proteins possess EF hand domains, which bind calcium and induce protein conformational shifts [27]. These shifts permit NCS members to interact in a calcium-dependent manner with specific target proteins.

For example, in photoreceptor cells, calcium activates recoverin and leads to the inhibition of rhodopsin kinase [28]. Additionally, conformational rearrangements can lead to the extrusion of a membrane-targeting myristoylation sequence, allowing for a calcium-induced change in protein localization [29]. Thus, NCS proteins are attractive candidates to perform activity-independent morphological changes in response to VGCC function.

We have previously described the role *C. elegans* VGCCs subunits *unc*-2, the neuronal P/Q-type α1 subunit, *and unc*-36, the auxiliary α2δ subunit, provide in synaptic morphology. Mutations in the conserved extracellular matrix molecule nidogen result in diffuse, elongated synaptic puncta [42], and this phenotype requires VGCC function [14]. Moreover, the VGCC regulatory role of *unc-2* and *unc-36* is specific to those subunits, as the other α1 subunits, *egl-19* and *cca-1*, and the second α2δ subunit, *tag-180*, encoded in the *C. elegans* genome did not suppress *nid-1* phenotype [14]. Here, we demonstrate a similar synaptic regulatory role for the EF hand containing protein CALM-1, which was identified through a *nid-1* suppressor screen.

calm-1 is the single ortholog of the vertebrate calcium- and integrin-binding proteins (CIB1-4), also known as calmyrin(1-4). CIB1 interacts with platelet-specific integrins [44, 45] and can function as a calcium-dependent ligand of $InsP_3Rs$ for both activation and inactivation of receptor function [46]. CIB1 is also capable of transporting sphingosine kinase 1 to the plasma membrane through its N-terminal myristoyl sequence [47]. CALM-1 performs a similar function in *C. elegans*, as it directs sphingosine kinase to the plasma membrane in cholinergic neurons [51].

CIB proteins are also localized in the nervous system, as CIB2 mRNA transcripts and protein are found in the hippocampus and cortex of rat brains [48]. Interestingly, CIB2 was recently discovered as a risk gene in patients with autism spectrum disorders [50]. Additionally, in cultured neurons, calmyrin1 has been shown to regulate neurite extension through stathmin2 (SCG10), and an *in vitro* microtubule polymerization assay showed calmyrin1 inhibits the microtubule-destabilizing effects of stathmin2 [49].

At *C. elegans* GABAergic NMJs, *calm-1* loss of function suppressed the synaptic defects present in *nid-1* mutants. Using a gain of function in *unc-2*, we found *calm-1* functioned downstream of UNC-2 VGCCs to regulate synaptic morphology. *calm-1* mutants did not have uncoordinated (Unc) locomotion, nor did they suppress the hyperactive locomotor activity present in *unc-2 (gof)* animals. These results are consistent with UNC-2 VGCCs affecting synaptic morphology independent of synaptic transmission. We also found the receptor for activated C kinase (RACK-1) bound CALM-1 in a calcium-dependent manner. Our work identifies *calm-1* as a novel effector of VGCC-dependent regulation of synaptic morphology. Our genetic analyses suggests a balance between VGCC-dependent regulation of morphology and synaptic adhesion that nidogen provides to allow for developmental synaptic growth to occur.

Section 3.3 Results

calm-1 is a suppressor of nidogen GABAergic neuromuscular junction defects

The D-type GABAergic motor neurons innervate the dorsal and ventral body wall muscles to help coordinate the characteristic sinusoidal movement of *Caenorhabditis elegans*. The neuromuscular junctions (NMJ) that are formed occur *en passant*, along the length of individual axons, leading to one neuron possessing multiple presynaptic areas (Fig. 3.1 A). We visualized NMJs using the presynaptic marker *juIs1* (*Punc-25::snb-1::*GFP), which labels synapses by expressing the synaptic vesicle protein synaptobrevin fused to GFP in GABAergic motor neurons [36, 37]. In wild-type (wt) young adult animals, SNB-1::GFP localized in discrete, evenly spaced puncta with an average of 0.82 ± 0.04 μm^2 (Fig. 3.1 B). We have previously described mutations in the genes encoding the *C. elegans* voltage-gated calcium channels (VGCC) subunits *unc-2* and *unc-36* suppress SNB-1::GFP accumulation defects associated with the extracellular matrix molecule (ECM) nidogen [14]. Despite the current understanding of VGCCs requirement in shaping synaptic morphology, the identification of downstream mediator molecules remains an area of active investigation.

We identified *calm-1* as a potential genetic modifier of *nid-1* in an RNAi-based screen (Tables 3.1 and 3.2). As *calm-1* contained calcium-binding motifs and a N-terminal myristoylation sequence, it was an ideal candidate to link changes in calcium concentration via VGCCs to the morphological architecture of NMJs (Fig. 3.2 A). We obtained a *calm-1 (lof)* allele*, tm1353,* which removes some of the 5' region adjacent to exon 1, exon 1 and part of the first intron (Fig. 3.2 B), and is likely a

complete null for *calm-1*. We visualized SNB-1::GFP puncta size in *nid-1(cg119);calm-1(tm1353)* of 1.09 ± 0.05 μm^2. Thus, *calm-1;nid-1* double mutants corroborated our RNAi by suppressing the elongated phenotype of nidogen mutants (Fig. 3.1 D). This was a significant decrease from 1.52 ± 0.13 μm^2 ($P < 0.05$) of *nid-1(cg119)* (Fig. 3.1 C). The *calm-1* single mutants also had an effect on SNB-1::GFP puncta size, with an area of 1.09 ± 0.06 μm^2 ($P <0.001$ versus wt and <0.05 versus *nid-1*) (Fig. 3.1 E). In contrast to the VGCC mutants, *unc-2* and *unc-36,* or the calmodulin kinase II mutant, *unc-43,* that we have previously described as *nid-1* suppressors [14], *calm-1* mutants do not have an uncoordinated (Unc) phenotype. This is consistent with our previous results that regulation of GABAergic NMJ morphology is, at least in part, due to mechanisms independent of vesicle exocytosis [14].

Synaptic defects of receptor tyrosine phosphatase, *ptp-3*, are suppressed by *calm-1*

Nidogen interacts with the receptor tyrosine phosphatase *ptp-3*/LAR to anchor the active zone protein SYD-2 (liprin-α) at the synapse [43]. Spanning from the extracellular matrix to the presynaptic active zone, this protein complex is positioned, and organized, to influence synaptic morphology. *ptp-3(mu256)* is a strong loss-of-function mutant [43], and results in the same diffuse, elongated SNB-1::GFP clusters as nidogen mutants, with synaptic areas averaging 1.52 ± 0.09 μm^2 ($P <0.001$ versus wt and $P >0.05$ versus *nid-1)* (Fig. 3.1 F). Since we observed *calm-1* mutations suppressed *nid-1* defects, we wondered if it would behave similarly in *ptp-3(mu256)* mutants. The *calm-1;ptp-3* double mutant suppressed these defects,

significantly reducing SNB-1::GFP cluster area to 0.78 ± 0.04 μm^2 (P <0.001 versus *ptp-3*) (Fig. 3.1 G). Previously, we observed similar effects using a mutation in *unc-36,* the extracellular VGCC α2/δ subunit, in combination with *ptp-3*, that is the doubles were more like *wt* than either of the single mutants [14]. Taken together, intact VGCCs and CALM-1 function are required for the defects associated with loss of the nidogen protein complex to be manifested.

calm-1 functions downstream of *unc-2* and *unc-36* to regulate neuromuscular junction morphology

calm-1 encodes an ortholog of the calcium-and integrin-binding proteins (CIB). Possessing three predicted calcium-binding EF hand motifs (EF hand 1 lacks an aspartate in position 1 of a canonical EF-hand, and thus it may not be a functional), CALM-1 can be classified as a neuronal calcium sensor (NCS) family member. NCS proteins undergo conformational changes after binding calcium membrane, allowing interactions with calcium-dependent target proteins [27]. One outcome of a conformational change in some NCS proteins, including calmyrin, is the protrusion of an N-terminal myristoylation modification, which drives proteins to the plasma membrane [29]. These characteristics make CALM-1 a candidate to be a downstream mediator of VGCC activity.

In *calm-1* mutants, along with suppressing the *nid*-1 mutation defects, SNB-1::GFP clusters were fewer in number, but larger in size than those in wild-type animals. VGCC subunits *unc-36* (1.23 ± 0.06 μm^2) and *unc-2* (1.26 ± 0.15 μm^2) have similar SNB-1 accumulation defects (Fig. 3.3 A,C). These results suggest the loss of

CALM-1 is akin, in regulating NMJ morphology, to the reduction of calcium entry through VGCCs. We tested if *calm-1* and the VGCC subunits worked redundantly or together to regulate SNB-1::GFP clusters. Double mutant analysis between *calm-1*;*unc-36* (1.30 ± 0.10 μm^2; P >0.05 versus *unc-36*; P >0.05 versus *calm-1*) and *calm-1;unc-2* (1.10 ± 0.7 μm^2; P >0.05 versus *calm-1*; P >0.05 versus *unc-2*) both displayed SNB-1::GFP cluster areas similar to each single mutant (Fig. 3.3 B,D). As the area of the puncta are well below the average size of puncta observed in other genotypes, it is unlikely that there is a threshold effect, and thus, we concluded these genes work in a common pathway to shape presynaptic domains.

One potential mechanism would involve calcium influx through VGCCs leading to activation of CALM-1, which initiates a secondary signaling cascade. Alternatively, CALM-1 could be acting upstream of VGCCs to augment calcium signaling by altering the properties of the channel, similar to Frequenin/NCS1 [86].

To understand the epistatic relationship between the VGCCs and CALM-1, a gain-of-function *(gof)* VGCC allele, *unc-2(zf35)*, was examined for synaptic defects [87]. Hyperactivation of UNC-2 resulted in abnormally large and irregularly shaped SNB-1::GFP clusters (1.75 ± 0.17 μm^2; P <0.001 versus wt; P <0.001 versus *calm-1*; P <0.05 versus *unc-2*), reminiscent of *nid-1* mutant puncta (Fig. 3.3 E). Removing CALM-1 from the *unc-2(zf35)* background reduced the SNB-1::GFP cluster area to 1.27 ± 0.07 μm^2 (P <0.05 versus *calm-1*; P >0.05 versus *unc-2* (*e55*)) (Fig. 3.3 F). This indicated CALM-1 was required for the SNB-1 accumulation defects observed in *unc-2(gof)* and, thus, likely operates downstream of UNC-2 in regulation of synaptic morphology. The *unc-2(zf35)* mutants exhibited a hyperactive locomotor

behavior, characterized by frequent backing with the average of 33 ± 1.6 reversals/min, a behavior not seen in wild-type animals (2 ± 0.25 reversals/min). The *calm-1(tm1353);unc-2(zf35)* animals had a similar behavioral phenotype to the *unc-2(zf35)* single mutants, with average of 22 ± 1.0 reversals/min (Fig. 3.3 H). This suggests that the activity of the UNC-2 channel was not grossly changed by the removal of *calm-1*, and that CALM-1 is unlikely to modify the activity of the channel. Overall we conclude from these results that *calm-1* is likely to function downstream of *unc-2*, independent of neurotransmission, to regulate synaptic morphology.

We next tested *unc-2(zf35);nid-1(cg119)* double mutants to understand the interaction between nidogen and hyperactivated voltage-gated calcium channels (Fig. 3.3 G). Double mutants have a SNB-1::GFP area of 1.71 ± 0.19 μm^2 ($P > 0.05$ versus), suggesting these two genes work in the same pathway to regulate synaptic morphology. Since we find that *nid-1* likely functions upstream of *unc-2,* and the *calm-1* mutation is able to suppress both *nid-1(cg119)* and *unc-2(zf35),* we conclude that the synaptic morphology defects in *nid-1(lof)* and *unc-2(gof)* are due to a common mechanism. A simple model is that NID-1 normally functions to inhibit synaptic growth, and that inhibition is relieved by activation of UNC-2. Since the *nid-1(cg119)* mutants do not cause a *zf35*-like locomotor activity, it is unlikely that NID-1 functions to inhibit UNC-2 activity in exocytosis.

CALM-1 localizes to the nervous system and musculature, and is required cell autonomously for proper neuromuscular junction morphology

We generated full-length CALM-1::GFP and RFP fusions to assay where the gene was expressed and the protein localized during development. The fusions were deemed functional since they partially rescued the egg-laying-defective (Egl) phenotype associated with *calm-1* animals (90% Egl for *tm1353* vs 35% for *tm1353;lhEx36;* data not shown). CALM-1::GFP was first detectable in embryos at the gastrula stage and expression persisted throughout development and into adulthood. CALM-1 appears to be highly expressed in the nervous system and musculature (Fig. 3.4 A-C). Within the muscle, CALM-1 appeared to be localized in puncta that appeared similar to the dense bodies, which are points of attachment between the actin cytoskeleton and ECM. CALM-1 also appeared in muscle arms, which extend from muscles to the nerve cord. In the nervous system, expression was seen in both GABAergic and cholinergic neurons (Fig. 3.5 A-C).

To test whether CALM-1 was functioning cell autonomously an N-terminally tagged mCherry::CALM-1 fusion protein was expressed under the *unc-25* promoter and introduced into the null mutant, *tm1353*. This construct rescued the SNB-1::GFP accumulation defects present in *tm1353*, resulting in puncta with an area of 0.88 $\mu m^2 \pm 0.06$ (Fig. 3.5 D) These results show that CALM-1 likely functioned in the VD neurons to regulate presynaptic morphology. We compared the subcellular localization of CALM-1::RFP relative to SNB-1::GFP clusters in the VD motor neurons. CALM-1::RFP was found throughout the VD neurons, with expression in the cell body, axon and localizing, partially, to GFP puncta. Similar to mCherry alone, CALM-1 was not specifically localized to synapses or the regions bordering synaptic

areas; rather, CALM-1 appears to be present diffusely throughout VD neurons, indicating is grossly localized to the cytoplasm under normal conditions.

The intracellular scaffolding molecule RACK-1 is a calcium-dependent binding partner of CALM-1

Our results suggested that *calm-1* could be part of a calcium-dependent signal downstream of UNC-2 to regulate changes in synaptic morphology. Since CALM-1 contains predicted EF hand motifs, we hypothesized CALM-1 could bind to target proteins in response to increased calcium at the synapse. We identified potential calcium-dependent interactions by incubating immobilized CALM-1 protein in the presence of calcium, then eluting bound proteins with EDTA.

We identified 14 proteins that interacted with CALM-1 in a calcium-dependent (Table 3.3). These proteins included multiple ribosomal subunit proteins, a eukaryotic initiation factor and the receptor for activated C kinase (RACK-1). RACK-1 was of interest because it is an intracellular scaffold involved in multiple neuronal processes [88] and functions in the GABA neurons to control axon pathfinding [89]. Interestingly, RACK-1 was found to interact with PTPμ both at cell contact points and to regulate E-cadherin-mediated adhesion [90, 91]. These data suggested to us that RACK-1 may interact in a similar manner in GABAergic synapse morphology.

We confirmed that CALM-1 and RACK-1 can physically interact *in vitro* in a calcium dependent fashion (Fig. 3.5 A). Next, we examined SNB-1::GFP patterning in *rack-1(tm2262),* which is a strong loss-of-function mutation in *rack-1* (Fig 3.5 B). The *tm2262* mutants displayed an increase in SNB-1::GFP cluster size, resulting in

areas of 1.65 ± 0.21 μm^2; P <0.001 versus wt (Fig. 3.5 C). The enlarged SNB-1::GFP clusters in *rack-1* mutants are suppressed by the removal of *calm-1* (1.18 ± 0.09 μm^2; P = 0.05 versus *rack-1*) (Fig. 3.5 D). Additionally, when RACK-1::GFP was expressed in the GABAergic motor neurons, it colocalized with another fluorescent synaptic-vesicle marker, RAB-3::mCherry (Fig. 3.5 E-G). Together, these results indicate RACK-1 is localized at presynaptic areas, and that regulates synapse morphology.

Section 3.4 Discussion

We have shown here CALM-1 plays a role in regulating GABAergic neuromuscular junction (NMJ) morphology in *C. elegans*. The *calm-1* locus encodes for an EF hand protein, and we have found that it interacts genetically in the same pathway as the voltage-gated calcium channel (VGCC) subunits UNC-2 and UNC-36 to regulate NMJ morphology. Genetic analysis suggests synaptic morphology regulation through VGCCs and CALM-1 contrasts with the role of the ECM component nidogen and the leukocyte-common antigen related receptor tyrosine phosphatase PTP-3. With these contrasting roles, calcium signaling components and cellular adhesion molecules work to provide a temporal switch that allows for synaptic stabilization and growth. This supports our previous results that demonstrate synapses form by elongation and division during development in an UNC-2-dependent manner.

calm-1 functions cell autonomously and downstream of VGCCs to regulate synaptic morphology

Nidogen and the tyrosine phosphatase PTP-3/LAR cooperate to anchor the active zone regulator liprin-α (SYD-2) at presynaptic areas [43]. The nature of this interaction likely provides an adhesive force that constricts synaptic material to discrete subcellular regions, as loss of function mutations result in a diffusion of synaptic puncta. We have previously shown mutations in *unc-2* and *unc-36* suppress the synaptic morphology defects associated with *nid-1* and *ptp-3*, indicating the elongated shape requires proper VGCC function [14].

Here, we find *calm-1*, which encodes a calcium-binding protein orthologous to the human calcium- and integrin-binding protein, acts cell autonomously and downstream of *unc-2* and *unc-36* to regulate NMJ morphology of *C. elegans* D-type GABAergic motor neurons. These data suggest CALM-1 links VGCC function with morphological changes at the synapse. Most work detailing VGCC function, regardless of system, has focused on its role in neuronal physiology and synaptic morphology, leaving the question of potential downstream molecules unresolved. One example of VGCC and calcium-binding protein interaction is at *Drosophila* NMJs. Frequenin/NCS-1 regulates presynaptic bouton number and synaptic firing through the α1 subunit *cacophony*, presumably activating VGCC to control morphology [86]. Thus, due to differences in organism, neuron type and calcium-binding properties, various calcium-binding proteins can act both upstream and downstream of VGCCs to regulate synaptic structure.

Interestingly, unlike mutations in *unc-2*, *unc-36* and other synaptic transmission mutants, *calm-1* mutants are not uncoordinated (Unc). And the suppression of the *unc-2(gof)* synaptic phenotype by *calm-1* mutants is not accompanied by the suppression of *unc-2(gof)* behavioral defects. By displaying a non-Unc behavioral phenotype with synaptic morphology defects, mutations in *calm-1* suggest it functions independent of neurotransmission to regulate synaptic structure. Supporting this, mutations in *unc-13*, required for synaptic transmission, do not have suppress defects in the shape of SNB-1::GFP puncta present in *nid-1* mutants [14, 36]. These results fit into recent accumulating evidence that synaptic structure can be regulated independent of synaptic firing [14, 15, 23, 24]. Taken

together, VGCCs also provide a role in developmental synaptic growth, involving distinct, or temporally regulated, molecules than activity-dependent synaptic growth.

Calcium signaling and its role in modulating synaptic adhesion

We are classifying genes with mutant phenotypes that result in enlarged, irregularly shaped puncta (*nid-1*, *rack-1, ptp-3,* and *unc-2(gof)*) as defective in synaptic adhesion; while the genes with mutant phenotypes that are enlarged but symmetrical shaped (*unc-2(lof)*, *calm-1* and *unc-36*). The *unc-2* mutants are also characterized by a failure to undergo normal elongation and division during development, suggesting they are defective in synapse expansion. We hypothesize synaptic adhesion and expansion exist in a balance that is regulated by temporal calcium signaling. First, the elongated mutant synaptic puncta resemble the intermediate stage of synaptic growth, regulated by *unc-2*, observed during wild-type *C. elegans* development [14]. This suggests proper calcium channel function is required for normal synaptic dynamics. Second, hyperactivated UNC-2 signaling mimics the synaptic defects of loss of molecules required for cellular adhesion, indicating that calcium channel function needs to be regulated for proper synaptic morphology. Finally, removing wild-type calcium signaling from adhesion mutants suppresses the associated elongated defects.

These results imply synaptic morphological changes require downregulation of synaptic adhesion molecules to initiate the diffusion of synaptic molecules into adjacent axonal regions. Accompanying downregulation of adhesion molecules, changes in intracellular calcium concentration activate secondary messengers that

finalize synapse expansion. The budding of synaptic areas then requires these changes in adhesion and calcium signaling to be reversed, to allow for new synapses to occur (Fig. 3.6).

Our genetic analysis suggests genes required for synapse expansion are epistatic to synapse adhesion molecules, as double mutants all suppress elongated phenotypes associated with adhesion genes. The calcium-dependent biochemical interaction between CALM-1 and RACK-1 may indicate a point where the switch in synaptic adhesion may occur. RACK-1 possesses seven WD40-repeat motifs, which allow it to interact with a diverse range of proteins [88]. Interestingly, calmodulin interacts with another WD-repeat protein, striatin, in neurons, and is responsible for striatin subcellular redistribution [92]. The CALM-1/RACK-1 interaction we see may operate in a similar manner.

Previous work has found *rack-1* works cell autonomously in the D-type motor neurons to control axon pathfinding [89]. We find *rack-1(lof)* mutants have enlarged SNB-1::GFP puncta in the D-type motor neurons, similar to *nid-1*, *ptp-3* and *unc-2(gof)* mutants. Moreover, like mutations in *nid-1*, *ptp-3* and *unc-2(gof)* mutants, *calm-1* was able to suppress the defects seen in *rack-1* mutants. These results indicate RACK-1 promotes synaptic adhesion similar to the extracellularly located NID-1 and the transmembrane protein PTP-3.

How would RACK-1 aid in synaptic adhesion? One possible way is by providing support for the PTP-3 and NID-1 adhesive complex. PTP-3 and NID-1 act to stabilize the synaptic organizing molecule SYD-2/liprin-α at synapses by residing in the plasma membrane and extracellular matrix, respectively [43]. RACK-1 may

act as a scaffolding molecule adjacent to the cell membrane to cluster liprin-α and other presynaptic components through the formation of multi-protein complexes. In cell culture, RACK-1 interacts with PTPμ at cell-cell contact points [91]. Further work looking at the interaction between RACK-1 and PTP-3, both in the presence and absence of CALM-1, at *C. elegans* NMJ would help provide insight into the molecular mechanisms of synaptic structural modulation.

A similar process of dynamic assembly and disassembly of synaptic areas occurs at *Drosophila* NMJs, involving the cellular adhesion molecule Fasciclin II (FasII). In this system, the specific amount of FasII determines synaptic bouton number in *Drosophila*, as null mutants have fewer boutons, compared with hypomorphic mutants that possess increased synaptic areas [93]. In contrast with the increase in synaptic growth of FasII mutants, synaptic activity is not altered [94]. These data indicate levels of FasII have a structural role in synaptic structural plasticity.

Moreover, *in vivo* time-lapse imaging of developing larvae found instances of lower levels of FasII at regions of synaptic connections that undergo a budding process that produces new synaptic boutons [52]. Additionally, FasII levels are reduced in the potassium channel double mutant *ether-a-go-go Shaker (eag Sh)*, which results in increased synaptic activity and bouton growth [94]. FasII levels are also reduced in hyperactivated CaMKII mutants that lead to increased synaptic bouton size, and are similar to loss-of-function mutations in synaptic scaffolding molecule Discs large (Dlg) [81]. Thus, synaptic bouton growth seems to require

CaMKII phosphorylation of Dlg, preventing Dlg from contacting FasII to stabilize synaptic areas.

In conclusion, the balance between synaptic stability and growth in the *C. elegans* GABAergic NMJs is modulated by the dynamic interactions that control either synaptic adhesion or expansion.

Section 3.5 Materials and Methods

Caenorhabditis elegans strains

All following strains were maintained at 20-22.5°C as previously described [83]. The following alleles and double mutants were used in this study: N2 (var. Bristol), *juIs1(Punc-25::*SNB-1::GFP), *calm-1(tm1353), rack-1(tm2262), unc-2(zf35), ptp-3(mu256), nid-1(cg119), unc-2(e55), unc-36(e251), calm-1(tm1353); unc-2(zf35), calm-1(tm1353);unc-36(e251), calm-1(tm1353);ptp-3(mu256), calm-1(tm1353);unc-2(zf35), calm-1(tm1353);rack-1(tm2262).* Transgenic animals were generated by germline transformation as previously described [84].

Molecular biology

A *calm-1* genomic fragment (including endogenous promoter) was amplified using pF30A10.1 F1 and F30A10.1 R1 to make pBA245 and recombined into (pDT57) to create P*calm-1*::CALM-1::GFP (pBA251). pBA251 was injected at 45ng/µL into *calm-1(tm1353)* to create EVL114 (lhEx36). (Building of construct and injection done by Dr. Brian Ackley.) To visualize if CALM-1 was localized in GABA neurons, P*calm-1*::CALM-1::tagRFP was generated by recombining pBA245 into pEVL334 (tag-RFP + let 858 3' UTR) using LR clonase Gateway System (Life technology) to create pEVL395. This was injected into *juIs1* at 10ng/µL to create EVL1001. A *calm-1* genomic fragment (minus endogenous promoter including the 3' UTR) was amplified using the following primers: *calm-1 ATG F1* and *calm-1 3'UTR R1*. This product was recombined into pEVL387 (*Punc-25::mCherry::unc-43 3' UTR*) by using the InFusion enzyme (Clontech) to generate pEVL408 (*Punc-*

25::mCherry::calm-1::calm-1 3′UTR). The pEVL408 plasmid was injected into *juIs1* animals at 10ng/µL to create EVL1204 (lhEx389), and crossed into *calm-1(tm1353);juIs1* to create EVL1218 for SNB-1::GFP colocalization analysis (Undergraduate Gavin Hanson crossed rescue construct into *tm1353* animals). RACK-1 and RAB-3 colocalization experiment was visualized by injecting pEVL26 (*Punc-25::mcherry::rab-3)* into *lqIs174* (P*unc-25::rack-1 gDNA::gfp)* at 5 ng/µL to create EVL352.

Image analysis

Neuromuscular junction morphology of GABAergic VD neurons was visualized by *juIs1* [*Punc-25* SNB-1::GFP]. All images were collected on an Olympus FV1000 confocal microscope equipped with Fluoview software. Images were acquired using multi-track parameters when necessary (*calm-1* rescue), with either a 60X Plan-apochromat objective. Animals were anesthetized using 0.5% phenoxy-propanol (TCI America) in M9 and mounted on 2% agarose pads. Measurements of SNB-1::GFP were as described, with minor modifications [42]. All images were collected using the exact same microscope settings. Briefly, confocal images were projected into a single plane using the maximum projection and exported as a tiff file with a scale bar. Using ImageJ the files were converted to a binary image using the threshold command, so that the binary image resembled the RGB image. A region of interest was drawn around SNB-1 puncta in the ventral nerve cord. The following measurement options were selected: Area, Center of Mass, Circularity, Perimeter, Fit Ellipse, and Limit to Threshold. Scaling was set by measuring the scale

bar. The “Analyze Particle” command was used with a minimum of four pixels and no maximum size. The following options were selected: Outline Particles, Ignore Particles Touching Edge, Include Interior Holes and Reset Counter. The resulting measurements were exported to Microsoft Excel for statistical analysis. Comparisons of single mutants and double mutants to the wild type, or specified genotype, were tested by Students two-tailed t-test.

Protein purification and CALM-1 pulldown:

calm-1 cDNA was recombined into pDEST17 using LR recombinase (Life Technologies) according to manufacturer’s directions to create pEVL25, and transformed into BL21(DE3) bacteria. Bacteria were grown to OD=600 and induced with 1mM IPTG for three hours at 37°C. Bacteria were collected by centrifugation and pellets frozen in liquid nitrogen. Pellets were lysed and dialyzed into binding buffer. 6His-CALM-1 was purified by affinity chromatography using nickel resin (Qiagen).

To collect animals for CALM-1 pulldown, N2 animals were grown on HB101; washed off plates with M9 and incubated with additional HB101, 500µL streptomycin (100µg/µL), 500µL of 5mg/ml cholesterol and M9 up to 500mL; shaken at room temperature for three days; liquid spun down and supernatant frozen and then lysed with worm lysis buffer (1xPBS, 10% glycerol, 0.1% NP40, 0.1% Tween 20 and 1mM PMSF). Solution was spun down and supernatant incubated with calcium binding buffer (20mM HEPES, 100mM KCL, 2mM $CaCl_2$, 0.1% NP-40, 0.1% Tween-20, pH 7.4) and incubated with CALM-1 column overnight. CALM-1 column was prepared by immobilizing to CNBr-activated sepharose beads

(GE Life Sciences; formerly Amersham Biosciences). Column was washed with calcium binding buffer, and interacting proteins were removed with 250μL of elution buffer (20mM HEPES, 100mM KCL, 5mM EDTA, 0.1% NP-40, 0.1% Tween-20, pH 7.4) Samples were concentrated by trichloroacetic acid (TCA) precipitation and run on a 7.5% SDS gel. Gel bands were excised and analyzed by MALDI-TOF mass spectrometry (University of Kansas MSPCL lab).

RACK-1 confirmation binding experiments:

A *calm-1* cDNA was recombined into pDEST15 and a *rack-1* cDNA was recombined into pDEST17 using LR recombinase (Life Technologies) according to manufacturer's directions and individually transformed into BL21(DE3) bacteria. Bacteria were grown to OD=600 and then proteins were induced with 1mM IPTG and grown overnight (16 hours) at 37 °C. Bacteria were collected by centrifugation and pellets frozen in liquid nitrogen. Pellets were lysed and dialyzed into binding buffer. GST-CALM-1 was purified by affinity chromatography using GST sepharose and 6-His-RACK-1 was purified via Ni++ resin.

Proteins were mixed at 1:1 mixture in phosphate buffer supplemented with EDTA or Ca2+ as indicated. Protein mixtures were purified via Ni2+ resin (Qiagen), and eluted using 300 mM imidazole according to manufacturer's directions. Flow through fractions were collected, and volumes of elution fractions were adjusted to be equal to the flow through. Elutions and flow through fractions were separated by SDS-PAGE and transferred to nylon membrane for western blotting. We probed for CALM-1 in the elution and flow through fractions using an anti-GST antibody. (Confirmation RACK-1 studies were conducted by Dr. Brian Ackley.)

Section 3.6 Figures

Figure 3.1

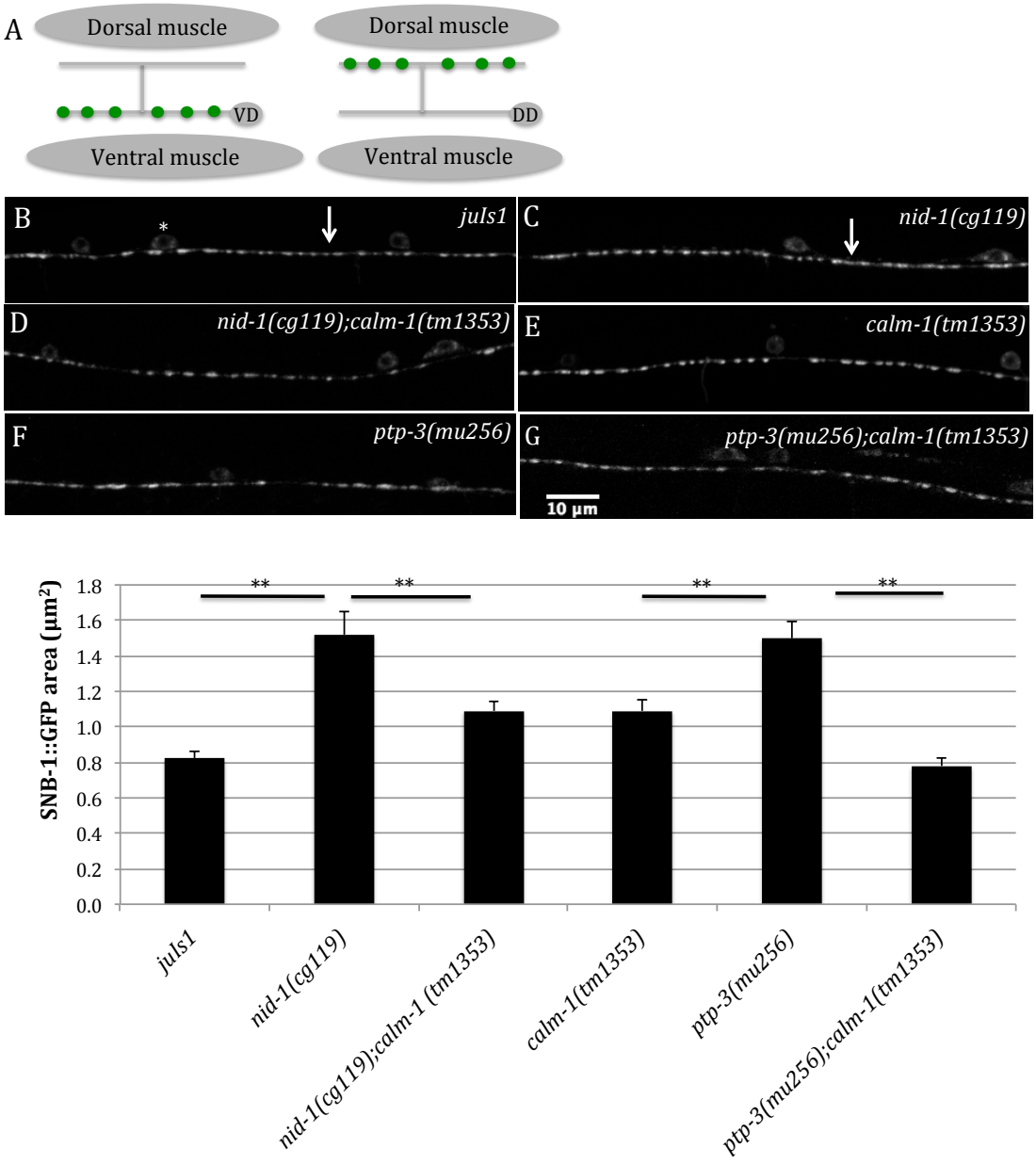

Figure 3.1 Synaptic defects associated with *nid-1* and *ptp-3* mutants are suppressed by *calm-1* (A) Schematic representation of D-type motor neurons. VD neurons have presynaptic areas (green circles) that innervate the ventral muscle wall; whereas DD neurons have their presynaptic areas that innervate the dorsal muscle wall. Cell bodies (blue circles) of both neurons reside in the ventral nerve cord. (B) Wild-type animals have punctate shaped SNB-1::GFP areas that are regular spaced along the nerve cord (arrow). Cell bodies are indicated by the asterisk. (C) *nid-1(cg119)* have elongated (arrows) and often irregularly shaped puncta (D) *calm-1(tm1353)* allele suppressed the defects observed in *nid-1* mutants. (E) *calm-1* mutants have enlarged synaptic areas when compared to *wt*. (F) *ptp-3* mutants show enlarged and disrupted SNB-1::GFP areas. (G) Removing *calm-1* from *ptp-3* rescued synaptic phenotype back to area seen in wild type. (H) Bar graph of SNB-1::GFP area. N>180 puncta; *P<0.05, **P<0.001. Statistical significance was calculated by using the Student's t-test. Error bars represent the Standard Error of the Mean (SEM).

Figure 3.2

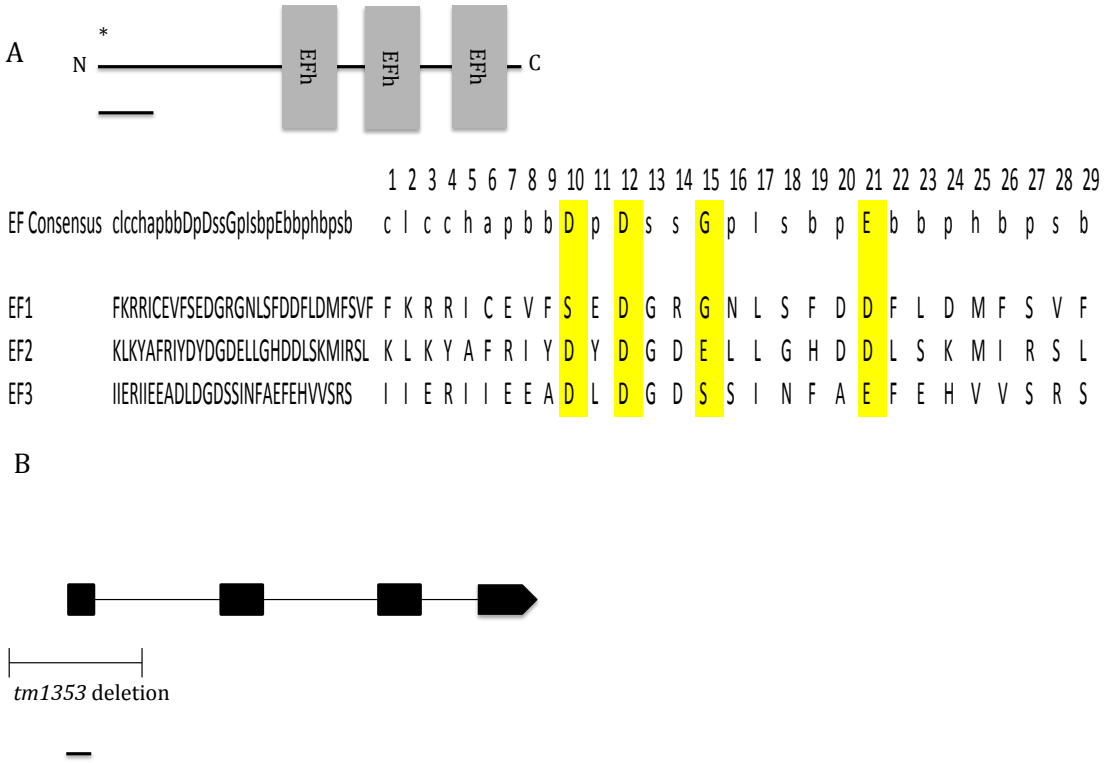
A
N
C
EFh
EFh
EFh
1 2 3 4 5 6 7 8 9 10 11 12 13 14 15 16 17 18 19 20 21 22 23 24 25 26 27 28 29
EF Consensus clcchapbbDpDssGplsbpEbbphbpsb c l c c h a p b b D p D s s G p l s b p E b b p h b p s b
EF1 FKRRICEVFSEDGRGNLSFDDFLDMFSVF F K R R I C E V F S E D G R G N L S F D D F L D M F S V F
EF2 KLKYAFRIYDYDGDELLGHDDLSKMIRSL K L K Y A F R I Y D Y D G D E L L G H D D L S K M I R S L
EF3 IIERIIEEADLDGDSSINFAEFEHVVSRS I I E R I I E E A D L D G D S S I N F A E F E H V V S R S
B
tm1353 deletion

Figure 3.2 *calm-1* encodes for a calcium binding protein (A) CALM-1 protein (201 amino acids) is an ortholog of the calcium- and integrin-binding proteins (also known as calmyrin). It has three predicted calcium-binding EF-hand motifs (As predicted by Simple Modular Architecture Research Tool (SMART): EF1 = 84-112; EF2 = 121-149; EF3 = 162-190), along with a putative myristoylation site (marked by asterisk) beginning at G2 of the protein. Sequence similarity computed as through PBIL Lyon-Gerland. Scale bar is equivalent to 25 amino acids. Positions highlighted in yellow indicate EF-hand conserved calcium binding residues. (B) The *calm-1* locus consists of four exons, and endogenous expression constructs contained 1.4kb of upstream sequence. The deletion allele *tm1353* removes the first coding exon, 5'UTR, and a portion of the first intron. It is believed to be a null mutant. Scale bar = 100bp.

Figure 3.3

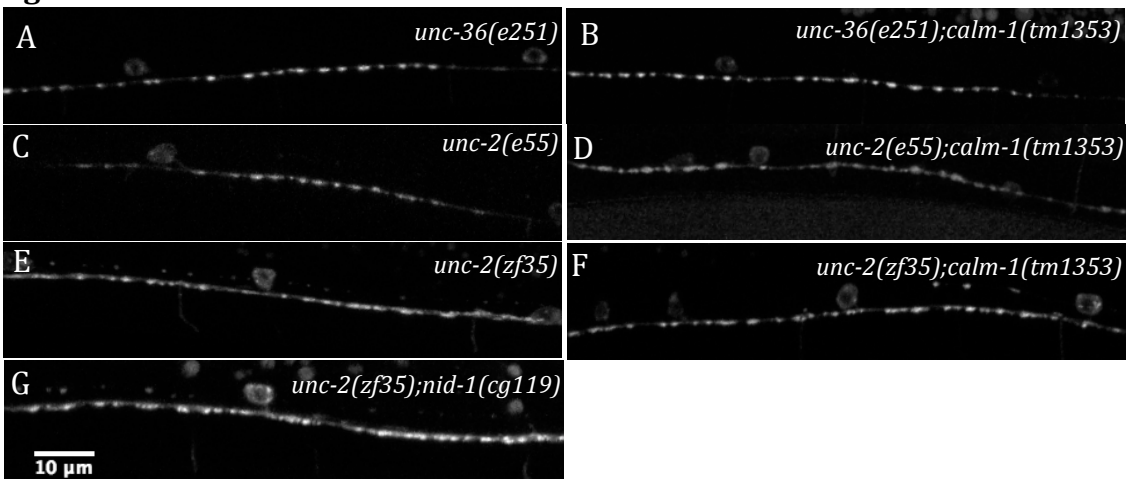
A
unc-36(e251)
B
unc-36(e251);calm-1(tm1353)
C
unc-2(e55)
D
unc-2(e55);calm-1(tm1353)
E
unc-2(zf35)
F
unc-2(zf35);calm-1(tm1353)
G
unc-2(zf35);nid-1(cg119)
10 µm

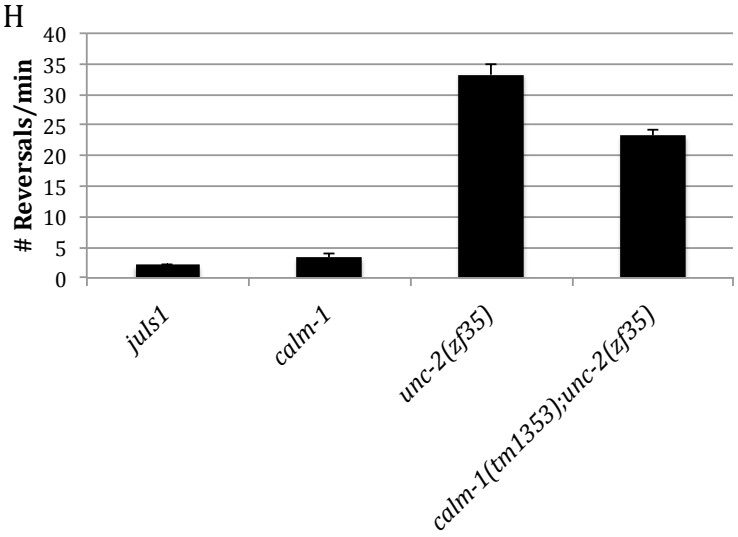
H
Reversals/min
0
5
10
15
20
25
30
35
40
juIs1
calm-1
unc-2(zf35)
calm-1(tm1353);unc-2(zf35)

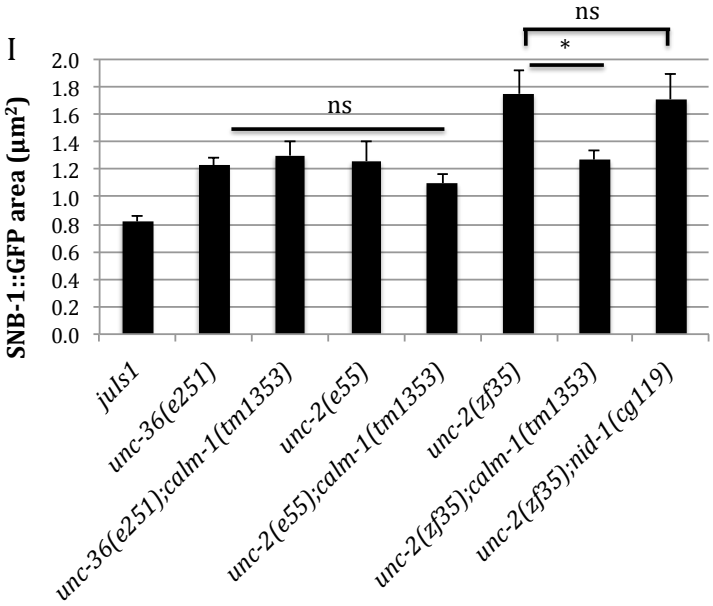
I
SNB-1::GFP area (µm²)
0.0
0.2
0.4
0.6
0.8
1.0
1.2
1.4
1.6
1.8
2.0
ns
*
ns
juIs1
unc-36(e251)
unc-36(e251);calm-1(tm1353)
unc-2(e55)
unc-2(e55);calm-1(tm1353)
unc-2(zf35)
unc-2(zf35);calm-1(tm1353)
unc-2(zf35);nid-1(cg119)

Figure 3.3 *calm-1* acts downstream of voltage-gated calcium channels in presynaptic morphology (A-D) *unc-36(e251)* (A) *and unc-2(e55)* (C) have enlarged synaptic areas compared to wild type. *unc-36* encodes for the α2δ subunit, and *unc-2* encodes for the α1 of the VGGCs. *unc-36; calm-1* (B) and *unc-2;calm-1* (D) double mutants show similar sizes compared to each single mutant, indicating they work in a similar pathway to regulate synaptic morphology. (E) An *unc-2* gain-of-function allele, (*zf35*), showed enlarged synaptic areas similar to *nid-1* mutants. (F) These defects were reduced in the loss-of-function *calm-1* mutant. (G) *unc-2(zf35); nid-1(cg119)* double mutants are not significantly increased from either single mutant (H) *unc-2(zf35)* hyperactive reversal behavior is reduced, but not completely suppressed by *calm-1*. Number of reversals averaged from 30 animals/genotype. (I) Bar graph of SNB-1::GFP area. N>180 puncta; *P<0.05. Statistical significance was calculated by using the Student's t-test. Error bars represent the Standard Error of the Mean (SEM).

Figure 3.4

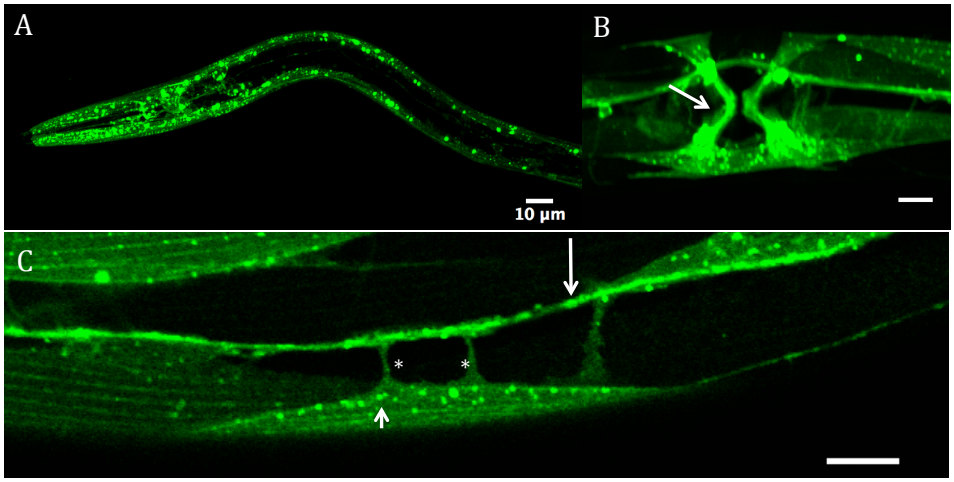

Figure 3.4 Expression of *calm-1* is observed ubiquitously and throughout development Panels are expressing P*calm-1*::CALM-1::GFP (A) Endogenous expression of *calm-1* is located ubiquitously throughout development, represented by expression in L1 animal. (B) Expression is also observed in vulva muscles of adult animals (arrows). (C) Majority of expression is observed in muscle and nervous system. Expression is seen in both muscle arms (asterisks) and dense bodies of the body wall muscles (arrowhead) and in the nerve cord (arrow). Unlabeled scale bars are 10μm.

Figure 3.5

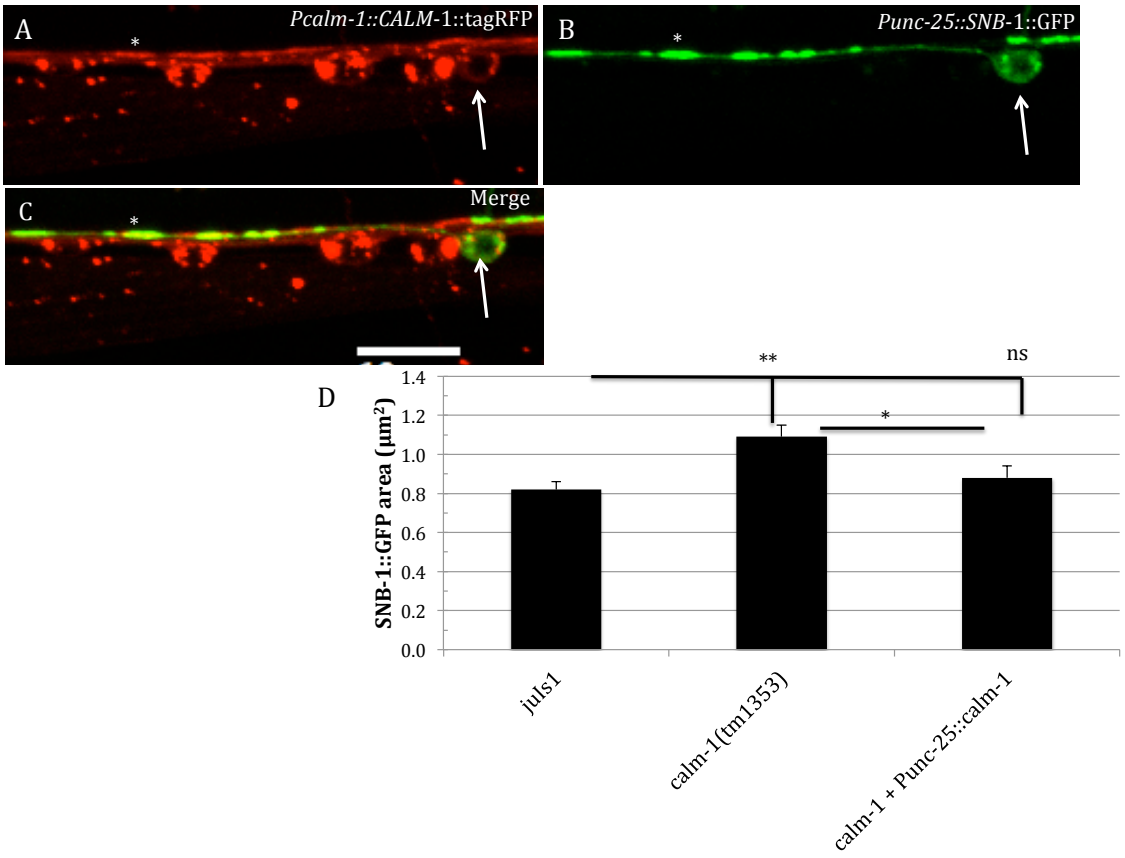
A
Pcalm-1::CALM-1::tagRFP
*
B
Punc-25::SNB-1::GFP
*
C
Merge
*
D
**
ns
*
SNB-1::GFP area (μm²)
1.4
1.2
1.0
0.8
0.6
0.4
0.2
0.0
juIs1
calm-1(tm1353)
calm-1 + Punc-25::calm-1

Figure 3.5 *calm-1* can function cell autonomously in GABAergic motor neurons to regulate synaptic morphology (A-C) Colocalization of CALM-1::RFP and SNB-1::GFP in GABAergic D-type neurons. *Pcalm-1::*CALM-1::tagRFP is localized in both cholinergic and GABAergic motor neurons. Its localization in the GABAergic motor neurons is identified by comparing its expression using the synaptic marker *juIs1.* The colocalization between *juIs1* and CALM-1 protein is observed in both cell bodies (arrow) and in regions with SNB-1::GFP (asterisk). Colocalization does appear at intersynaptic regions. (D) P*unc-25*::mCherry::CALM-1 expression in GABA neurons was able to rescue SNB-1::GFP defect of *calm-1* mutants. Bar graph of SNB-1::GFP area. N>180 puncta; *P<0.05, **P<0.001. Statistical significance was calculated by using the Student's t-test. Error bars represent the Standard Error of the Mean (SEM). Scale bar is 10μm**.**

Figure 3.6

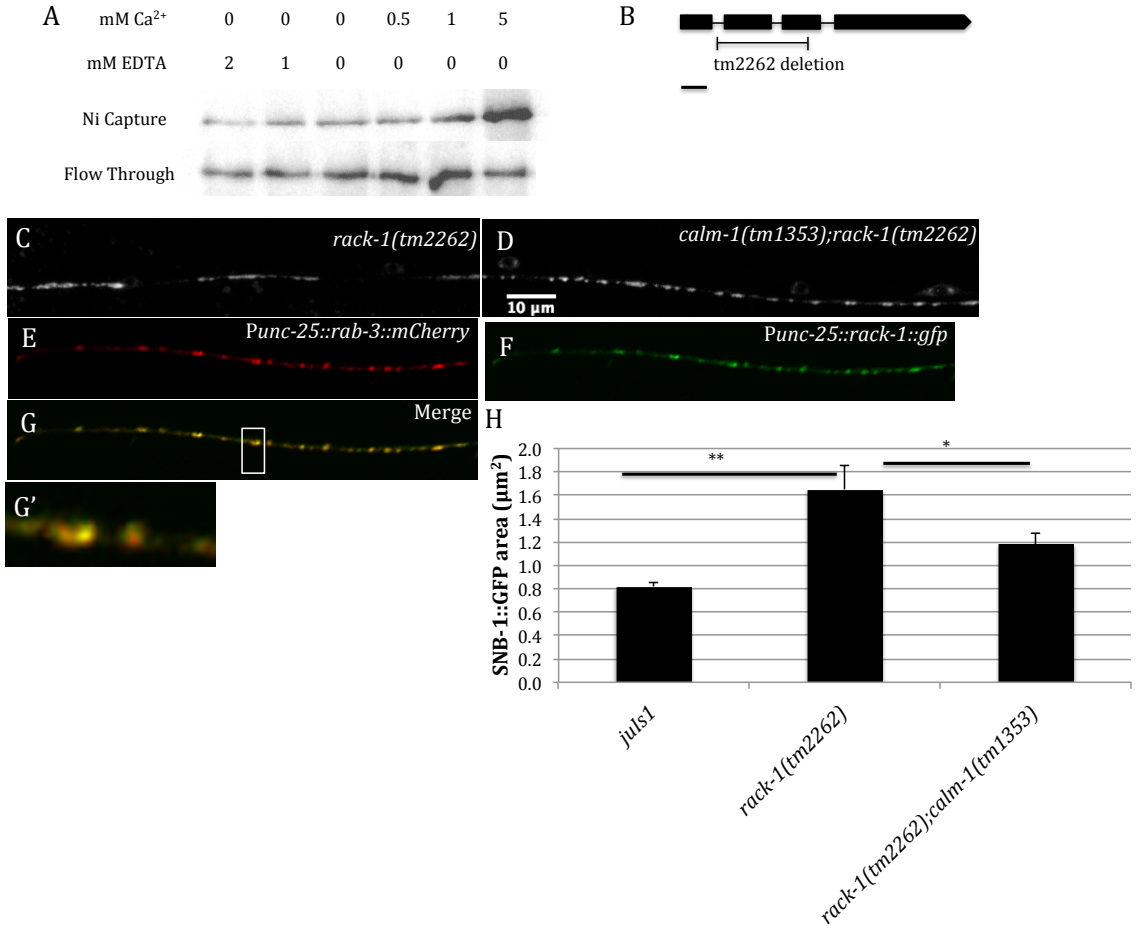
A
mM Ca2+ 0 0 0 0.5 1 5
mM EDTA 2 1 0 0 0 0
Ni Capture
Flow Through
B
tm2262 deletion
C
rack-1(tm2262)
D
calm-1(tm1353);rack-1(tm2262)
10 µm
E
Punc-25::rab-3::mCherry
F
Punc-25::rack-1::gfp
G
Merge
G'
H
SNB-1::GFP area (µm2)
2.0
1.8
1.6
1.4
1.2
1.0
0.8
0.6
0.4
0.2
0.0
**
*
juIs1
rack-1(tm2262)
rack-1(tm2262);calm-1(tm1353)

Figure 3.6 *rack-1* phenocopies *nid-1* synaptic defects, and is suppressed reduced with loss of *calm-1* (A) 6-His-RACK-1 and GST-CALM-1 were mixed at an equimolar ratio in increasing concentrations of calcium. After purifying 6-His-RACK-1 using Ni^{2+}-agarose, we probed for GST-CALM-1 using an anti-GST antibody. We found that RACK-1 and CALM-1 can physically interact in a calcium-dependent manner (B) Gene structure of *rack-1*. The *tm2262* allele has an in frame deletion that is likely a strong loss of function. (C) Similar to *nid-1*, *rack-1(tm2262)* shows increased SNB-1::GFP areas, having both elongated and malformed puncta. (D) The defects observed in *rack-1* mutants were reduced in *calm-1;rack-1* double mutants (E-G) RACK-1 colocalized with the synaptic vesicle marker RAB-3 (H) Bar graph of SNB-1::GFP area. N>180 puncta; *P=0.05, **P<0.001. Statistical significance was calculated by using the Student's t-test. Error bars represent the Standard Error of the Mean (SEM).

Figure 3.7

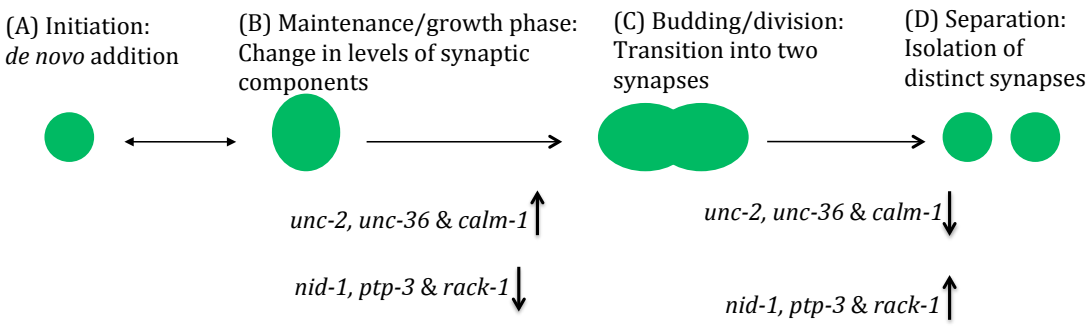
(A) Initiation:
de novo addition
(B) Maintenance/growth phase:
Change in levels of synaptic components
(C) Budding/division:
Transition into two synapses
(D) Separation:
Isolation of distinct synapses
unc-2, unc-36 & calm-1
nid-1, ptp-3 & rack-1
unc-2, unc-36 & calm-1
nid-1, ptp-3 & rack-1

Figure 3.7 Model of developmental synaptic growth (A) Synapses are established *de novo* and exist in a homeostasis. (B) In response to unidentified growth signal, presynaptic areas start to increase in size. The increase in size is governed by calcium signaling and a reduction in nidogen-mediated adhesion, which drives expansion of synaptic areas to an intermediate stage. (C) Enlarged synaptic areas, once again in response to an unidentified signal, reverse to a more adhesive state, which requires a decrease in calcium signaling and increase in nidogen-mediated adhesion. (D) The end result of this process is the establishment of two synaptic connections from a single preexisting synapse. This secondary mechanism of synapse growth, supplementing *de novo* addition, may help provide a rapid increase in synapses that must accompany organismal growth.

Section 3.7 Tables

Table 3.1 Enhancers of *nid-1(cg119)* synaptic phenotype

Gene	Brief description
acd-1	Acid sensitive Degenerin
D2092.1	C2 calcium-binding motif-containing protein
W04A4.4	Calpain thiol protease
asic-2	Acid-sensing/Amiloride-Sensitive Ion Channel family; mechanosensory protein like
F46A8.7	Unknown function
best-26	Bestrophin (chloride channel) homolog
ncs-2	Ca2+ sensor (EF-Hand superfamily); neuronal calcium sensor
spp23	Saposin-like protein family
dapk-1	Death associated protein kinase homolog – ankryin and protein kinase
eva-1	Enhancer of unc-40 ventral axon guidance defects

*List of confirmed enhancers of *nid-1* synaptic phenotype. Genes were identified in an RNAi screen looking for modifiers of the enlarged SNB-1::GFP puncta observed in *nid-1(cg119)* animals. Genes of interest first identified by knockdown that resulted in qualitatively larger puncta, followed by confirmation of enhancement through measuring synaptic areas.

Table 3.2 Suppressors of *nid-1(cg119)* synaptic phenotype

Gene	Brief description
mks-6	C2 calcium-binding motif-containing protein
calm-1	Calcium- and integrin-binding protein
W04A8.2	Unknown function
ipgm-1	Phosphoglycerate mutase
fbxa-217	F-box containing protein

*List of confirmed suppressors of *nid-1* synaptic phenotype. Genes were identified in an RNAi screen looking for modifiers of the enlarged SNB-1::GFP puncta observed in *nid-1(cg119)* animals. Genes of interest first identified by knockdown that resulted in qualitatively smaller puncta, followed by confirmation of suppression through measuring synaptic areas.

Table 3.3 CALM-1 interacting proteins from calcium-dependent pulldown

Gene	Brief description
rack-1	Receptor of Activated C Kinase
eif-6	Eukaryotic initiation factor
hsp-70	Heat shock protein
rps-6	Small (40S) ribosomal subunit S6 protein
rpl-2	Large ribosomal subunit L8 protein
rpl-7A	Large ribosomal subunit L7a protein
rsp-3	SR protein, splicing factor
rpl-5	Large ribosomal subunit L5 protein
rpl-4	Large ribosomal subunit L4 protein
rpa-0	Acidic ribosomal subunit protein P0
lec-1	Galectin

Chapter IV
Concluding remarks and future directions

Section 4.1 Concluding remarks

The findings in chapter II reveal the role of VGCCs in regulating presynaptic morphology at a distinct developmental time point. Specifically, time-lapse microscopy suggests UNC-2 is required for synaptic growth that occurs during the L4 larval stage of *C. elegans*. It is important to note while the time-lapse studies in this dissertation examine synaptic dynamics during the L4 larval stage, we do not rule out the possibility of UNC-2 functioning earlier in development for synaptic growth. Regardless, the synaptic growth observed in L4 larval animals seems to require the modification (presumably inhibition) of cellular adhesion, since wild-type animals have a higher prevalence of *nid-1*-like SNB-1::GFP puncta. Furthermore, the increased average area of SNB-1::GFP puncta in late L4 animals is not retained in young adult animals, indicating synaptic adhesion may need to be upregulated to refine elongated puncta to a smaller size.

These data are consistent with a dynamic process of synaptic growth that cycles between loss of adhesion to expand current synaptic areas, followed by increased adhesion to facilitate budding from the enlarged L4 puncta to produce the smaller puncta observed in young adults. We believe this process of expansion and budding of existing synapses occurs alongside *de novo* addition of synapses to ensure the proper number of synaptic connections is established during increased organismal growth.

Chapter III identifies a calcium-binding protein, CALM-1, that genetically interacts downstream of VGCCs to cell autonomously regulate presynaptic morphology, a novel finding for the calmyrin family of proteins. Additionally, a

CALM-1 calcium-dependent pulldown identified the intracellular scaffolding molecule RACK-1 as a potential target of CALM-1, in response to VGCC activity. The increased synaptic area of *rack-1* loss-of-function mutants indicates it restricts synaptic growth in a manner similar to *nid-1*, although it remains unclear if it acts together or redundantly with *nid-1*. It is currently unknown how, or if, the CALM-1/RACK-1 interaction specifically affects synaptic morphology. But the genetic and biochemical data suggest CALM-1/RACK-1 may function as a molecular switch that facilitates the change from synaptic stability to growth.

Our genetic analyses, overall, indicate two categories of synaptic defects observed in this dissertation: loss-of-function mutations in *unc-2, unc-36* and *calm-1* have enlarged and organized puncta, while *nid-1, rack-1, ptp-3* and *unc-2(gof)* mutants displayed elongated and disorganized puncta. Additionally, *unc-2, unc-36* or *calm-1* suppress defects of *nid-1, rack-1, unc-2(gof)* and *ptp-3*. These results invoke a genetic model of synaptogenesis where NID-1 (and phenotypically related genes) inhibits calcium-dependent synaptic growth (Fig. 4.1). Coupled with results from the developmental analysis of synaptic puncta from chapter II, we hypothesize a balance between synaptic adhesion and calcium signaling to control developmentally regulated synaptogenesis.

In conclusion, the results presented here reveal a calcium pathway that regulates the addition of presynaptic areas during *C. elegans* development. Both the characterization of UNC-2-mediated synaptic dynamics and the identification of CALM-1 augment the current knowledge of synaptic biology by characterizing a

developmentally sensitive period of synapse addition reliant on VGCCs, in addition to identifying a downstream effector to regulate synaptic morphology.

Section 4.2 Future Directions

The findings presented in this dissertation provide new insights into synaptic biology, but also raise additional questions about synaptic growth at *C. elegans* GABAergic NMJs. Going forward, addressing the following questions will further illuminate the nature of the previously described synaptic dynamics.

Question 1: How is RACK-1 functioning at GABAergic NMJs?

In chapter III, RACK-1 was demonstrated to bind CALM-1 in a calcium-dependent manner, and *rack-1* mutants displayed increased synaptic areas that were suppressed by *calm-1*. The genetic studies are consistent with RACK-1 functioning to promote synaptic adhesion, but it is unknown if it works together with NID-1 to do so. The physical interaction between CALM-1 and RACK-1 may suggest a point of convergence between calcium signaling and synaptic adhesion. We hypothesize RACK-1 works with the NID-1 complex, and acts as a switch between the adhesive and expansionary states at the synapse in response to UNC-2 activity.

Synaptic areas of the *rack-1;nid-1* double mutant would identify if *rack-1* worked in the *nid-1* pathway. We predict synaptic areas would be similar to both single mutants, indicating a common pathway to regulate synaptic morphology. Despite both of these single mutants having significantly enlarged areas from wild-type animals, our prediction is not based on reaching a synaptic-area ceiling; *unc-36* loss-of-function mutants increase the already enlarged and disorganized areas of collagen XVIII, *cle-1* (unpublished data).

We believe RACK-1 functions through the NID-1 complex because of cell culture evidence demonstrating RACK-1 binds PTPμ, which may suggest a similar interaction at GABAergic NMJs. For example, RACK-1 binds the catalytic phosphatase domain of PTPμ, and these proteins interact at the points of cell-cell contacts in MvLu cells grown at high density [91]. Furthermore, this interaction was inhibited by constitutively activate *src*, indicating protein competition can disrupt RACK-1/PTPμ binding [91]. RACK-1 also interacts with PTPμ in LNCaP prostate carcinoma cells, where PTPμ expression induces E-cadherin-mediated adhesion [90]. Thus, RACK-1 and PTP-3 may be interacting at the presynaptic membrane of GABAergic NMJs to promote synaptic adhesion, and this interaction could be disrupted by CALM-1 binding to RACK-1 (Fig. 4.2).

The phosphatase activity of PTP-3 is required for the proper formation of synapses in the GABA neurons [43]. Thus, regulating the phosphorylation state of active zone proteins could result in a control mechanism that can switch from synaptic adhesion to growth. Since *rack-1* phenocopies *ptp-3*, we hypothesize RACK-1 stabilizes PTP-3 at the synapse. We predict the disruption of phosphatase activity by a potential CALM-1/RACK-1 interaction could be achieved by altering PTP-3 levels.

If RACK-1 stabilizes PTP-3, we may be able to detect this effect by examining any deviations in PTP-3 localization using the PTP-3A::GFP marker strain, *juIs194*. If RACK-1 stabilizes PTP-3, then mutations in *calm-1* may increase PTP-3 intensity since CALM-1 is not present to disrupt RACK-1 interaction with PTP-3; conversely, *rack-1* mutants would result in decreased intensity of PTP-3A::GFP. We would

confirm the CALM-1/RACK-1 interaction affects PTP-3 activity by reintroducing both enzymatic inactive and active copies of PTP-3 into *unc-2(gof)*.

If hyperactive calcium signaling is modulating PTP-3 phosphatase activity, overexpressing phosphatase active copies of PTP-3 may suppress the elongated SNB-1::GFP puncta in *unc-2(gof)*. If suppression occurred, we expect enzymatically inactive PTP-3 to have no effect. Alternatively, enzymatically inactive PTP-3 may suppress the *unc-2(gof)* phenotype. This result suggests PTP-3 can also structurally regulate synaptic morphology, and is disrupted by CALM-1 interacting with RACK-1.

Question 2: Does the postsynaptic muscle contribute to the regulation of synaptic growth during development?

While the work in this dissertation focuses exclusively on presynaptic regulation of synapse morphology, our analysis would not be complete if we did not investigate the contribution, if any, the postsynaptic muscle cells make in shaping GABAergic NMJs. For example, do the muscles signal to GABA neurons to regulate synapse morphology? Also, is there a coordinated developmental program between neurons and muscle that dictates synaptic dynamics during *C. elegans* development?

We first are interested in understanding the role of the GABA receptor, UNC-49, in regulating synaptic morphology. *unc-49(e407)* mutant animals possess SNB-1::GFP puncta that are similar in shape and size as loss-of-function mutations in *unc-2* and *unc-36* (Fig. 4.3), suggesting an effect on presynaptic areas due to lack of GABA receptor since the *e407* is a null allele of *unc-49*.

The defects are not believed to be caused by loss of GABA transmission since GABA synthesis mutants, *unc-25*, and mutants unable to undergo synaptic vesicle fusion, *unc-13*, do not have morphology defects [14, 36]. These results are similar, but not identical, to what is seen in *C. elegans* SAB NMJs, where loss of postsynaptic cholinergic receptor *unc-29* in muscle cells, as well as a gain-of-function mutation in the potassium channel *egl-36*, leads to sprouting of cholinergic presynaptic areas that is similar to defects in presynaptic neurotransmission [95].

We would make *calm-1;unc-49* double mutants to determine how UNC-49 regulates GABAergic synapses, since *calm-1* mutants do not have an uncoordinated phenotype and regulate synaptic morphology downstream of VGCCs. If there is genetic redundancy between *unc-49* and *calm-1*, we would expect to find an increase in synaptic areas of the double mutant. *unc-49* redundancy with *calm-1* would suggest a separate pathway through which UNC-49 shapes synaptic morphology. Conversely, presynaptic areas of similar size to each single mutant would be observed if UNC-49 regulates morphology similarly to CALM-1 and the VGCCs. Likewise, the *unc-49;nid-1* double mutant would be expected to suppress the defects of *nid-1*, similar to *unc-2;nid-1* and *calm-1;nid-1*.

Ordering the sequence of any coordination between muscle and neuron synaptic dynamics would also prove to be informative. UNC-49 is located on the muscle arms that contact motor neuron axons, and receptor clusters are observed in a 1:1 ratio to presynaptic SNB-1::GFP puncta [36, 40]. This localization positions it to affect or mirror presynaptic morphology. Looking at receptor clustering in the genetic backgrounds of our interest, UNC-49 immunostaining of *juIs1* (wild type),

unc-2(gof) and *calm-1(lof)* show a 1:1 ratio of UNC-49 to SNB-1, but only in puncta that resemble wild-type size (Fig. 4.4). Interestingly, this is similar to what is seen with synaptic organizing molecule SYD-2 localization in elongated SNB-1::GFP puncta. SYD-2 normally localizes to a single, discrete punctum surrounded by a larger accumulation of SNB-1::GFP [96]. But mutations in *rpm-1,* an E3 ubiquitin ligase, result in enlarged SNB-1::GFP that possess an increased number, not size, of SYD-2 puncta [96].

These results suggests there is a size limitation of active zones, and neurons overcome this limitation by adding new active zones to regions of enlarged presynaptic areas, which might instruct the formation of new UNC-49 clusters. We hypothesize there is a temporal relationship between the increase in UNC-49 clusters and enlarged presynaptic areas, and predict the enlargement of existing SNB-1::GFP areas precedes the accumulation of UNC-49 puncta.

Two lines of evidence indicate the elongation of SNB-1::GFP might precede the appearance of UNC-49 puncta. First, muscle arms extend and synapse onto ectopic axons that terminate before reaching the dorsal nerve cord, and also extend to the synaptic vesicle-rich cell bodies in animals with mutations in the kinesin gene *unc-104* [97, 98]. Secondly, UNC-49 clusters appear after initial SNB-1::GFP formation, and these clusters form opposite of GABA release sites on ectopic axonal projections [40]. Interestingly, receptor clustering is not dependent on neurotransmission, as clustering is normal in *unc-25* mutants [40]. This supports the hypothesis of a neuronal clustering factor, independent of GABA signaling, that informs UNC-49 receptor localization.

These studies were performed in L1 animals, and it is unknown if the mechanism of GABA receptor clustering is similar for synapses added later during development. Indeed, the majority of muscle arm extension occurs between the L1 and L2 developmental stage [99], which is before the time period we observed synaptic growth dynamics [14].

To determine if UNC-49 receptor clustering precedes SNB-1::GFP puncta elongation during the wild-type L4 larval stage, an UNC-49 fusion protein will be expressed in tandem with our SNB-1::GFP marker. Time-lapse microscopy will be utilized to simultaneously observe receptor clustering alongside presynaptic dynamics. UNC-49 clusters are predicted to appear after SNB-1::GFP elongation, supporting the neuronal clustering factor hypothesis.

Alternatively, UNC-49 clusters could precede SNB-1::GFP expansion, presumably because of the existence of muscle arms in the region. This would not be totally unexpected because ectopic muscle cells, resulting from ablation of muscle precursor cells, possess the ability to attract motor neuron processes, leading to ectopic branches and sprouting of GABAergic NMJs [100]. Hence, muscles possess the ability to influence synapse formation. This would fall in line with results from *Drosophila* NMJ, where CaMKII regulates presynaptic morphology from the postsynaptic muscle [81, 101]. Regardless of the origin of the initiating signal, either result would provide exciting insight into the mechanism of synaptic addition during growth.

Section 4.3 Figures

Figure 4.1

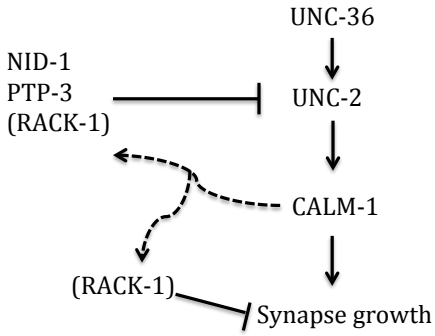

Figure 4.1 Model of genetic interactions that regulate synaptic growth Genetic analyses of synaptic morphology suggests a mechanism to regulate synaptic growth. Data from *unc-2* gain-of-function (*gof*) animals suggests calcium signaling is required for synaptic growth, as SNB-1::GFP puncta areas are increased in these mutants. Further evidence implicating calcium signaling in promoting growth comes from *unc-2*, *unc-36* and *calm-1* mutant suppression of the increased synaptic areas observed in *nid-1, ptp-3, rack-1*, and *unc-2 (gof)* mutants. These data support a model where NID-1 complex restricts synaptic growth by inhibiting calcium signaling through UNC-2. Relief of NID-1 complex inhibition results in synapse growth. Genetic analysis suggests RACK-1 also inhibits synapse growth, but it is unknown if it is through the NID-1/PTP-3 complex or another parallel pathway. The calcium-dependent interaction of CALM-1 and RACK-1 may have an impact on RACK-1 inhibition.

Figure 4.2

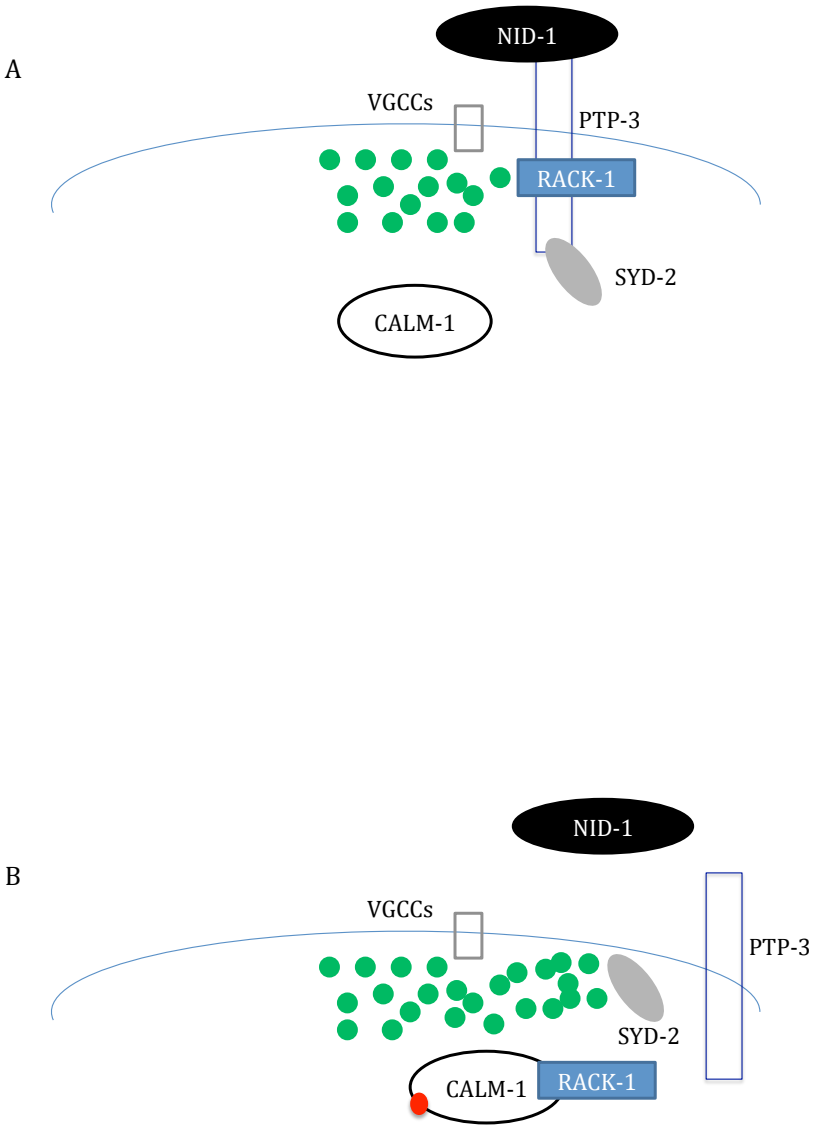
A
NID-1
VGCCs
PTP-3
RACK-1
SYD-2
CALM-1
B
NID-1
VGCCs
PTP-3
SYD-2
CALM-1
RACK-1

Figure 4.2 Potential molecular model of developmental synapse growth A simplified model of synapse addition through existing synaptic contacts may occur. (A) Prior to calcium entry, the nidogen adhesion complex exists by connecting the extracellular matrix to synaptic organizing molecule, SYD-2. We hypothesize that RACK-1 aids in the stability of the adhesion complex by interacting with PTP-3. (B) Calcium entry through VGCCs activates CALM-1 (red circle). In response to activation, CALM-1 binds RACK-1 and alters the PTP-3/NID-1 complex (either enzymatically or structurally), leading to the diffusion of SYD-2 and expansion of synaptic areas.

Figure 4.3

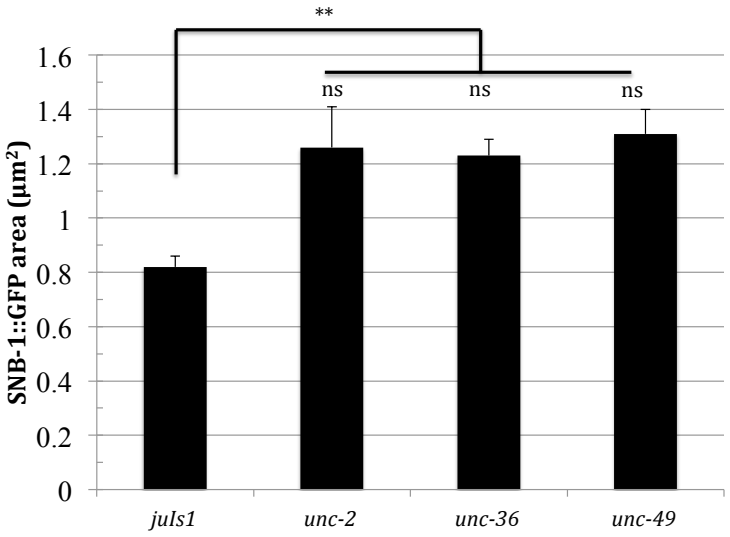
**
ns
ns
ns
1.6
1.4
1.2
1
0.8
0.6
0.4
0.2
0
SNB-1::GFP area (µm²)
juls1
unc-2
unc-36
unc-49

Figure 4.3 UNC-49 mutants possess enlarged SNB-1::GFP puncta Bar graph of SNB-1::GFP area comparing wild type to *unc-2*, *unc-36* and *unc-49* mutants. A loss-of-function mutation in the GABA receptor, *unc-49*, phenocopies loss-of-function mutations in VGCC subunits *unc-2* and *unc-36*. All three possess significantly increased SNB-1::GFP areas compared to wild type, while not significantly differing from each other. N>180 puncta; **P<0.01. Statistical significance was calculated by using the Student's t-test. Error bars represent the Standard Error of the Mean (SEM). Confocal image acquisition and image analysis were conducted as previously described in chapters II and III.

Figure 4.4

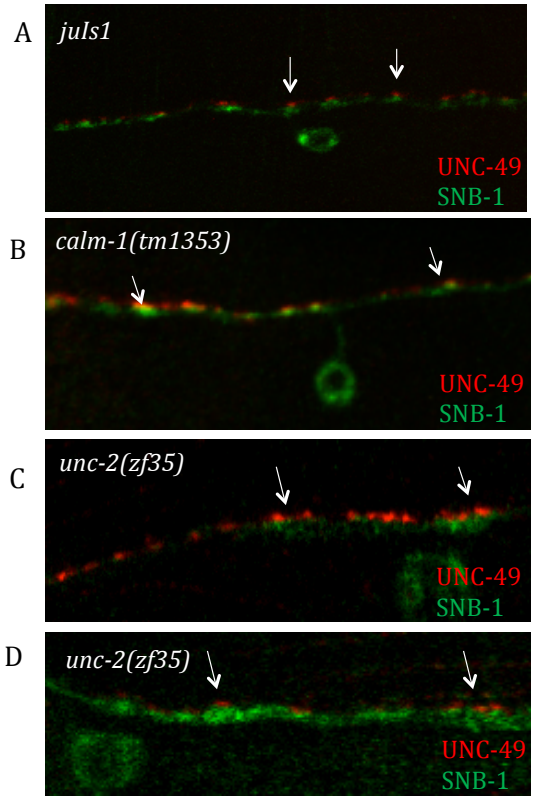
A
juIs1
UNC-49
SNB-1
B
calm-1(tm1353)
UNC-49
SNB-1
C
unc-2(zf35)
UNC-49
SNB-1
D
unc-2(zf35)
UNC-49
SNB-1

Figure 4.4 UNC-49 puncta align, up to a certain size, with SNB-1::GFP puncta Visualization of GABA receptors via antibody staining of various *juIs1* (wild type) genotypes with rabbit anti-UNC-49 primary antibody (3:1000) and Alexa 594-labeled anti-rabbit secondary antibody (1:10,000). (A) Wild-type animals (*juIs1*) have UNC-49 puncta across from SNB-1::GFP puncta (arrows) (B) *calm-1(tm1353)* animals also have UNC-49 receptors across from SNB-1::GFP puncta (arrows). (C-D) *unc-2(zf35)* animals have receptor clusters that are not equivalent in size to SNB-1::GFP puncta. Some enlarged SNB-1::GFP areas have multiple receptor clusters (arrows).

References

1. Tau, G. and B. Peterson, *Normal development of brain circuits.* Neuropsychopharmacology : official publication of the American College of Neuropsychopharmacology, 2010. **35**(1): p. 147-168.
2. Sudhof, T.C., *The presynaptic active zone.* Neuron, 2012. **75**(1): p. 11-25.
3. Kennedy, M., *Signal-processing machines at the postsynaptic density.* Science (New York, N.Y.), 2000. **290**(5492): p. 750-754.
4. Yamagata, M., J.R. Sanes, and J.A. Weiner, *Synaptic adhesion molecules.* Curr Opin Cell Biol, 2003. **15**(5): p. 621-32.
5. Kano, M. and K. Hashimoto, *Synapse elimination in the central nervous system.* Curr Opin Neurobiol, 2009. **19**(2): p. 154-61.
6. Stettler, D.D., et al., *Axons and synaptic boutons are highly dynamic in adult visual cortex.* Neuron, 2006. **49**(6): p. 877-87.
7. Yang, G., F. Pan, and W.-B. Gan, *Stably maintained dendritic spines are associated with lifelong memories.* Nature, 2009. **462**(7275): p. 920-924.
8. Xu, T., et al., *Rapid formation and selective stabilization of synapses for enduring motor memories.* Nature, 2009. **462**(7275): p. 915-919.
9. Duman, R.S. and G.K. Aghajanian, *Synaptic Dysfunction in Depression: Potential Therapeutic Targets.* Science, 2012. **338**.
10. Chu, Y., et al., *Enhanced synaptic connectivity and epilepsy in C1q knockout mice.* Proceedings of the National Academy of Sciences of the United States of America, 2010. **107**(17): p. 7975-7980.
11. Waites, C.L. and C.C. Garner, *Presynaptic function in health and disease.* Trends Neurosci, 2011. **34**(6): p. 326-37.
12. Catterall, W.A., *Voltage-gated calcium channels.* Cold Spring Harb Perspect Biol, 2011. **3**(8): p. a003947.
13. Catterall, W.A., *Structure and regulation of voltage-gated Ca2+ channels.* Annu Rev Cell Dev Biol, 2000. **16**: p. 521-55.
14. Caylor, R.C., Y. Jin, and B.D. Ackley, *The Caenorhabditis elegans voltage-gated calcium channel subunits UNC-2 and UNC-36 and the calcium-dependent kinase UNC-43/CaMKII regulate neuromuscular junction morphology.* Neural Dev, 2013. **8**: p. 10.
15. Rieckhof, G.E., et al., *Presynaptic N-type calcium channels regulate synaptic growth.* J Biol Chem, 2003. **278**(42): p. 41099-108.
16. Richmond, J., R. Weimer, and E. Jorgensen, *An open form of syntaxin bypasses the requirement for UNC-13 in vesicle priming.* Nature, 2001. **412**(6844): p. 338-341.
17. Schafer, W.R. and C.J. Kenyon, *A calcium-channel homologue required for adaptation to dopamine and serotonin in Caenorhabditis elegans.* Nature, 1995. **375**(6526): p. 73-8.
18. Mathews, E.A., et al., *Critical residues of the Caenorhabditis elegans unc-2 voltage-gated calcium channel that affect behavioral and physiological properties.* J Neurosci, 2003. **23**(16): p. 6537-45.

19. Kawasaki, F., R. Felling, and R.W. Ordway, *A temperature-sensitive paralytic mutant defines a primary synaptic calcium channel in Drosophila.* J Neurosci, 2000. **20**(13): p. 4885-9.
20. Saheki, Y. and C.I. Bargmann, *Presynaptic CaV2 calcium channel traffic requires CALF-1 and the alpha(2)delta subunit UNC-36.* Nat Neurosci, 2009. **12**(10): p. 1257-65.
21. Ly, C.V., et al., *straightjacket is required for the synaptic stabilization of cacophony, a voltage-gated calcium channel alpha1 subunit.* J Cell Biol, 2008. **181**(1): p. 157-70.
22. Dickman, D.K., P.T. Kurshan, and T.L. Schwarz, *Mutations in a Drosophila alpha2delta voltage-gated calcium channel subunit reveal a crucial synaptic function.* J Neurosci, 2008. **28**(1): p. 31-8.
23. Kurshan, P.T., A. Oztan, and T.L. Schwarz, *Presynaptic alpha2delta-3 is required for synaptic morphogenesis independent of its Ca2+-channel functions.* Nat Neurosci, 2009. **12**(11): p. 1415-23.
24. Eroglu, C., et al., *Gabapentin receptor alpha2delta-1 is a neuronal thrombospondin receptor responsible for excitatory CNS synaptogenesis.* Cell, 2009. **139**(2): p. 380-92.
25. Berridge, M.J., P. Lipp, and M.D. Bootman, *The versatility and universality of calcium signalling.* Nat Rev Mol Cell Biol, 2000. **1**(1): p. 11-21.
26. Chin, D. and A. Means, *Calmodulin: a prototypical calcium sensor.* Trends in cell biology, 2000. **10**(8): p. 322-328.
27. Burgoyne, R.D., *Neuronal calcium sensor proteins: generating diversity in neuronal Ca2+ signalling.* Nat Rev Neurosci, 2007. **8**(3): p. 182-93.
28. Chen, C.K., et al., *Ca(2+)-dependent interaction of recoverin with rhodopsin kinase.* J Biol Chem, 1995. **270**(30): p. 18060-6.
29. O'Callaghan, D.W., et al., *Differential use of myristoyl groups on neuronal calcium sensor proteins as a determinant of spatio-temporal aspects of Ca2+ signal transduction.* J Biol Chem, 2002. **277**(16): p. 14227-37.
30. Ackley, B.D. and Y. Jin, *Genetic analysis of synaptic target recognition and assembly.* Trends Neurosci, 2004. **27**(9): p. 540-7.
31. Margeta, M.A., K. Shen, and B. Grill, *Building a synapse: lessons on synaptic specificity and presynaptic assembly from the nematode C. elegans.* Curr Opin Neurobiol, 2008. **18**(1): p. 69-76.
32. White, J., et al., *The structure of the nervous system of the nematode Caenorhabditis elegans.* Philosophical transactions of the Royal Society of London. Series B, Biological sciences, 1986. **314**(1165): p. 1-340.
33. Shaye, D. and I. Greenwald, *OrthoList: a compendium of C. elegans genes with human orthologs.* PloS one, 2011. **6**(5).
34. Brose, N., et al., *Mammalian homologues of Caenorhabditis elegans unc-13 gene define novel family of C2-domain proteins.* The Journal of biological chemistry, 1995. **270**(42): p. 25273-25280.
35. Hata, Y., C. Slaughter, and T. Südhof, *Synaptic vesicle fusion complex contains unc-18 homologue bound to syntaxin.* Nature, 1993. **366**(6453): p. 347-351.

36. Jin, Y., et al., *The Caenorhabditis elegans gene unc-25 encodes glutamic acid decarboxylase and is required for synaptic transmission but not synaptic development.* J Neurosci, 1999. **19**(2): p. 539-48.
37. Hallam, S. and Y. Jin, *lin-14 regulates the timing of synaptic remodelling in Caenorhabditis elegans.* Nature, 1998. **395**(6697): p. 78-82.
38. Jorgensen, E., et al., *Defective recycling of synaptic vesicles in synaptotagmin mutants of Caenorhabditis elegans.* Nature, 1995. **378**(6553): p. 196-199.
39. Jorgensen, E.M. and M.L. Nonet, *Neuromuscular junctions in the nematode C. elegans.* Seminars in Developmental Biology, 1995. **6**.
40. Gally, C. and J.L. Bessereau, *GABA is dispensable for the formation of junctional GABA receptor clusters in Caenorhabditis elegans.* J Neurosci, 2003. **23**(7): p. 2591-9.
41. White, J.G., et al., *The structure of the ventral nerve cord of Caenorhabditis elegans.* Philos Trans R Soc Lond B Biol Sci, 1976. **275**(938): p. 327-48.
42. Ackley, B.D., et al., *The basement membrane components nidogen and type XVIII collagen regulate organization of neuromuscular junctions in Caenorhabditis elegans.* J Neurosci, 2003. **23**(9): p. 3577-87.
43. Ackley, B.D., et al., *The two isoforms of the Caenorhabditis elegans leukocyte-common antigen related receptor tyrosine phosphatase PTP-3 function independently in axon guidance and synapse formation.* J Neurosci, 2005. **25**(33): p. 7517-28.
44. Yuan, W., et al., *CIB1 is an endogenous inhibitor of agonist-induced integrin alphaIIbbeta3 activation.* J Cell Biol, 2006. **172**(2): p. 169-75.
45. Tsuboi, S., *Calcium integrin-binding protein activates platelet integrin alpha IIbbeta 3.* J Biol Chem, 2002. **277**(3): p. 1919-23.
46. White, C., et al., *CIB1, a ubiquitously expressed Ca2+-binding protein ligand of the InsP3 receptor Ca2+ release channel.* J Biol Chem, 2006. **281**(30): p. 20825-33.
47. Jarman, K.E., et al., *Translocation of sphingosine kinase 1 to the plasma membrane is mediated by calcium- and integrin-binding protein 1.* J Biol Chem, 2010. **285**(1): p. 483-92.
48. Blazejczyk, M., et al., *Biochemical characterization and expression analysis of a novel EF-hand Ca2+ binding protein calmyrin2 (Cib2) in brain indicates its function in NMDA receptor mediated Ca2+ signaling.* Archives of biochemistry and biophysics, 2009. **487**(1): p. 66-78.
49. Sobczak, A., et al., *Calmyrin1 binds to SCG10 protein (stathmin2) to modulate neurite outgrowth.* Biochim Biophys Acta, 2011. **1813**(5): p. 1025-37.
50. Prasad, A., et al., *A discovery resource of rare copy number variations in individuals with autism spectrum disorder.* G3 (Bethesda, Md.), 2012. **2**(12): p. 1665-1685.
51. Chan, J.P. and D. Sieburth, *Localized sphingolipid signaling at presynaptic terminals is regulated by calcium influx and promotes recruitment of priming factors.* J Neurosci, 2012. **32**(49): p. 17909-20.
52. Zito, K., et al., *Watching a synapse grow: noninvasive confocal imaging of synaptic growth in Drosophila.* Neuron, 1999. **22**(4): p. 719-29.

53. Catterall, W., et al., *International Union of Pharmacology. XLVIII. Nomenclature and structure-function relationships of voltage-gated calcium channels.* Pharmacological reviews, 2005. **57**(4): p. 411-425.
54. Dalton, S., et al., *A single CaVbeta can reconstitute both trafficking and macroscopic conductance of voltage-dependent calcium channels.* The Journal of physiology, 2005. **567**(Pt 3): p. 757-769.
55. Opatowsky, Y., et al., *Structural analysis of the voltage-dependent calcium channel beta subunit functional core and its complex with the alpha 1 interaction domain.* Neuron, 2004. **42**(3): p. 387-399.
56. De Jongh, K., C. Warner, and W. Catterall, *Subunits of purified calcium channels. Alpha 2 and delta are encoded by the same gene.* The Journal of biological chemistry, 1990. **265**(25): p. 14738-14741.
57. Andrade, A., et al., *Proteolytic cleavage of the voltage-gated Ca2+ channel alpha2delta subunit: structural and functional features.* Eur J Neurosci, 2007. **25**(6): p. 1705-10.
58. Felix, R., *Voltage-dependent Ca2+ channel alpha2delta auxiliary subunit: structure, function and regulation.* Receptors Channels, 1999. **6**(5): p. 351-62.
59. Nishimune, H., J. Sanes, and S. Carlson, *A synaptic laminin-calcium channel interaction organizes active zones in motor nerve terminals.* Nature, 2004. **432**(7017): p. 580-587.
60. Richmond, J., R. Weimer, and E. Jorgensen, *An open form of syntaxin bypasses the requirement for UNC-13 in vesicle priming.* Nature, 2001.
61. Weimer, R., et al., *UNC-13 and UNC-10/rim localize synaptic vesicles to specific membrane domains.* The Journal of neuroscience : the official journal of the Society for Neuroscience, 2006. **26**(31): p. 8040-8047.
62. Carlson, S., G. Valdez, and J. Sanes, *Presynaptic calcium channels and α3-integrins are complexed with synaptic cleft laminins, cytoskeletal elements and active zone components.* Journal of neurochemistry, 2010. **115**(3): p. 654-666.
63. Chen, J., S. Billings, and H. Nishimune, *Calcium channels link the muscle-derived synapse organizer laminin β2 to Bassoon and CAST/Erc2 to organize presynaptic active zones.* The Journal of neuroscience : the official journal of the Society for Neuroscience, 2011. **31**(2): p. 512-525.
64. Schafer, W., B. Sanchez, and C. Kenyon, *Genes affecting sensitivity to serotonin in Caenorhabditis elegans.* Genetics, 1996.
65. Frøkjaer-Jensen, C., et al., *Effects of voltage-gated calcium channel subunit genes on calcium influx in cultured C. elegans mechanosensory neurons.* Journal of neurobiology, 2006. **66**(10): p. 1125-1139.
66. Lainé, V., et al., *The alpha1 subunit EGL-19, the alpha2/delta subunit UNC-36, and the beta subunit CCB-1 underlie voltage-dependent calcium currents in Caenorhabditis elegans striated muscle.* The Journal of biological chemistry, 2011. **286**(42): p. 36180-36187.
67. Hunt-Newbury, R., et al., *High-throughput in vivo analysis of gene expression in Caenorhabditis elegans.* PLoS biology, 2007. **5**(9).

68. Kang, S. and J. Kramer, *Nidogen is nonessential and not required for normal type IV collagen localization in Caenorhabditis elegans.* Molecular biology of the cell, 2000.
69. Davies, A., et al., *Functional biology of the alpha(2)delta subunits of voltage-gated calcium channels.* Trends in pharmacological sciences, 2007. **28**(5): p. 220-228.
70. Tran-Van-Minh, A. and A. Dolphin, *The alpha2delta ligand gabapentin inhibits the Rab11-dependent recycling of the calcium channel subunit alpha2delta-2.* The Journal of neuroscience : the official journal of the Society for Neuroscience, 2010. **30**(38): p. 12856-12867.
71. Colbran, R. and A. Brown, *Calcium/calmodulin-dependent protein kinase II and synaptic plasticity.* Current opinion in neurobiology, 2004. **14**(3): p. 318-327.
72. Lisman, J., R. Yasuda, and S. Raghavachari, *Mechanisms of CaMKII action in long-term potentiation.* Nature reviews. Neuroscience, 2012. **13**(3): p. 169-182.
73. Tam, T., et al., *Voltage-gated calcium channels direct neuronal migration in Caenorhabditis elegans.* Developmental biology, 2000. **226**(1): p. 104-117.
74. Umemura, T., P. Rapp, and C. Rongo, *The role of regulatory domain interactions in UNC-43 CaMKII localization and trafficking.* Journal of cell science, 2005. **118**(Pt 15): p. 3327-3338.
75. Reiner, D., et al., *Diverse behavioural defects caused by mutations in Caenorhabditis elegans unc-43 CaM kinase II.* Nature, 1999. **402**(6758): p. 199-203.
76. Park, E. and H. Horvitz, *Mutations with dominant effects on the behavior and morphology of the nematode Caenorhabditis elegans.* Genetics, 1986. **113**(4): p. 821-852.
77. Woo, J., et al., *Trans-synaptic adhesion between NGL-3 and LAR regulates the formation of excitatory synapses.* Nature neuroscience, 2009. **12**(4): p. 428-437.
78. Johnson, K., et al., *The HSPGs Syndecan and Dallylike bind the receptor phosphatase LAR and exert distinct effects on synaptic development.* Neuron, 2006. **49**(4): p. 517-531.
79. Hoogenraad, C.C., et al., *Liprinalpha1 degradation by calcium/calmodulin-dependent protein kinase II regulates LAR receptor tyrosine phosphatase distribution and dendrite development.* Dev Cell, 2007. **12**(4): p. 587-602.
80. Beumer, K., et al., *Integrins regulate DLG/FAS2 via a CaM kinase II-dependent pathway to mediate synapse elaboration and stabilization during postembryonic development.* Development, 2002.
81. Koh, Y., et al., *Regulation of DLG localization at synapses by CaMKII-dependent phosphorylation.* Cell, 1999.
82. Fox, M., et al., *A synaptic nidogen: developmental regulation and role of nidogen-2 at the neuromuscular junction.* Neural development, 2008. **3**: p. 24.
83. Brenner, S., *The genetics of Caenorhabditis elegans.* Genetics, 1974. **77**(1): p. 71-94.

84. Mello, C.C., et al., *Efficient gene transfer in C.elegans: extrachromosomal maintenance and integration of transforming sequences.* EMBO J, 1991. **10**(12): p. 3959-70.
85. Dolphin, A.C., *A short history of voltage-gated calcium channels.* Br J Pharmacol, 2006. **147 Suppl 1**: p. S56-62.
86. Dason, J.S., et al., *Frequenin/NCS-1 and the Ca2+-channel alpha1-subunit co-regulate synaptic transmission and nerve-terminal growth.* J Cell Sci, 2009. **122**(Pt 22): p. 4109-21.
87. Schumacher, J., et al., *Intercellular calcium signaling in a gap junction-coupled cell network establishes asymmetric neuronal fates in C. elegans.* Development (Cambridge, England), 2012. **139**(22): p. 4191-4201.
88. Sklan, E.H., E. Podoly, and H. Soreq, *RACK1 has the nerve to act: structure meets function in the nervous system.* Prog Neurobiol, 2006. **78**(2): p. 117-34.
89. Demarco, R.S. and E.A. Lundquist, *RACK-1 acts with Rac GTPase signaling and UNC-115/abLIM in Caenorhabditis elegans axon pathfinding and cell migration.* PLoS Genet, 2010. **6**(11): p. e1001215.
90. Hellberg, C.B., et al., *Expression of the receptor protein-tyrosine phosphatase, PTPmu, restores E-cadherin-dependent adhesion in human prostate carcinoma cells.* J Biol Chem, 2002. **277**(13): p. 11165-73.
91. Mourton, T., et al., *The PTPmu protein-tyrosine phosphatase binds and recruits the scaffolding protein RACK1 to cell-cell contacts.* J Biol Chem, 2001. **276**(18): p. 14896-901.
92. Bartoli, M., A. Monneron, and D. Ladant, *Interaction of calmodulin with striatin, a WD-repeat protein present in neuronal dendritic spines.* J Biol Chem, 1998. **273**(35): p. 22248-53.
93. Schuster, C.M., et al., *Genetic dissection of structural and functional components of synaptic plasticity. I. Fasciclin II controls synaptic stabilization and growth.* Neuron, 1996. **17**(4): p. 641-54.
94. Schuster, C.M., et al., *Genetic dissection of structural and functional components of synaptic plasticity. II. Fasciclin II controls presynaptic structural plasticity.* Neuron, 1996. **17**(4): p. 655-67.
95. Zhao, H. and M.L. Nonet, *A retrograde signal is involved in activity-dependent remodeling at a C. elegans neuromuscular junction.* Development, 2000. **127**(6): p. 1253-66.
96. Zhen, M., et al., *Regulation of presynaptic terminal organization by C. elegans RPM-1, a putative guanine nucleotide exchanger with a RING-H2 finger domain.* Neuron, 2000. **26**(2): p. 331-43.
97. Hedgecock, E., J. Culotti, and D. Hall, *The unc-5, unc-6, and unc-40 genes guide circumferential migrations of pioneer axons and mesodermal cells on the epidermis in C. elegans.* Neuron, 1990. **4**(1): p. 61-85.
98. Hall, D. and E. Hedgecock, *Kinesin-related gene unc-104 is required for axonal transport of synaptic vesicles in C. elegans.* Cell, 1991. **65**(5): p. 837-847.
99. Dixon, S.J. and P.J. Roy, *Muscle arm development in Caenorhabditis elegans.* Development, 2005. **132**(13): p. 3079-92.

100. Plunkett, J.A., R.B. Simmons, and W.W. Walthall, *Dynamic interactions between nerve and muscle in Caenorhabditis elegans.* Dev Biol, 1996. **175**(1): p. 154-65.
101. Haghighi, A.P., et al., *Retrograde control of synaptic transmission by postsynaptic CaMKII at the Drosophila neuromuscular junction.* Neuron, 2003. **39**(2): p. 255-67.